

AN ITALIAN SCIENCE CASE FOR LOFAR

Coordinated by :

Gianfranco Brunetti¹

Contributions by :

Enzo Branchini², Gianfranco Brunetti¹, Carlo Burigana³,
Ettore Carretti¹, Rossella Cassano¹, Daniela Crociani⁴,
Luigina Feretti¹, Andrea Ferrara⁵, Marcello Giroletti¹,
Karl-H. Mack¹, Mauro Messerotti⁶, Lauro Moscardini⁴,
Matteo Murgia⁷, Andrea Possenti⁷, Isabella Prandoni¹,
Tiziana Venturi¹, Matteo Viel⁶

¹ INAF IRA, via P.Gobetti 101, Bologna

² Dip. Fisica, Univ. di Roma III, via della Vasca Navale 84, Roma

³ INAF IASF, via P.Gobetti 101, Bologna

⁴ Dip. Astronomia, Univ. di Bologna, via Ranzani 1, Bologna

⁵ SISSA, via Beirut 4, Trieste

⁶ INAF Oss. Astr. di Trieste, via G.B. Tiepolo 11, Trieste

⁷ INAF Oss. Astr. di Cagliari, Poggio dei Pini, Str.54, Capoterra

Contents

1	LOFAR	1
2	Cosmology with LOFAR	3
2.1	The Cosmic Dark Ages and Reionization	3
2.2	The Cosmic Dark Ages at 21 cm	4
2.3	21 cm temperature fluctuations and the structure formation	11
2.4	Alcock-Paczyński test at high redshift with the 21cm line	13
2.5	Structure formation at high redshift in non standard cosmological scenarios	15
3	Extragalactic Surveys	21
3.1	Survey plans	21
3.2	Scientific Perspective of LOFAR Extragalactic surveys	21
3.3	Deep LOFAR Fields and the Benefits of International Baselines	22
3.3.1	The AGN component	23
3.3.2	The starburst galaxies component	25
4	Radio Galaxies and Quasars	29
4.1	Energetics & Spectrum of particles	29
4.2	Relativistic Jets	29
4.2.1	Jet Structure	30
4.2.2	Blazars	31
4.3	Radio Hot Spots & low energy electron cut-off	31
4.3.1	Hot spots as ideal e-LOFAR targets	32
4.4	Giant radio sources	33

4.5	Dying Radio sources	35
4.5.1	The last phase in the life of a radio source	35
4.5.2	The spectral evolution of dying sources	36
4.5.3	Dying sources in low-frequency surveys	36
4.5.4	The impact of LOFAR	37
5	Galaxy Clusters	39
5.1	Radio Halos and Relics	39
5.2	Radio Surveys of Galaxy Clusters	41
5.3	The Ultra-Steep-Spectrum Radio Halos	43
5.4	Broad band non thermal cluster emission and synergies with observations in other bands	45
5.5	Thomson scattering of a cluster central radio source	47
5.5.1	Multifrequency complementarity	49
5.5.2	Polarization	50
6	Large Scale Magnetic Fields	51
6.1	Introduction	51
6.2	Observational diagnostics of magnetic fields	52
6.2.1	Synchrotron diffuse emission	52
6.2.2	Rotation measure	52
6.3	Magnetic fields in clusters	53
6.4	Magnetic fields in the intergalactic medium	55
6.5	Origin of intracluster magnetic fields	56
6.6	Magnetic field studies with LOFAR and eLOFAR	57
6.7	Summary of the LOFAR and eLOFAR specifications	58
7	Studies of the Galactic Magnetism	61
7.1	Magnetic fields probes at radio wavelengths	61
7.2	The Galactic Magnetic Field	63

7.3	Galactic magnetism at low frequencies: LOFAR	65
8	Radio Pulsar Studies	69
8.1	Scientific Case	69
8.2	The impact of Lofar on pulsar research	69
8.3	The case for a single station	73
9	Solar-Terrestrial Physics with LOFAR	75
9.1	Introduction	75
9.2	Low-Frequency Radio Diagnostics of Solar Phenomena	76
9.2.1	Solar Radio Bursts	76
9.2.2	Solar and Interplanetary Plasma Turbulence	78
9.3	Low-Frequency Radio Diagnostics of Heliospheric Phenomena	78
9.4	Low-Frequency Radio Diagnostics of the Earth's Ionosphere	78
9.5	Conclusions	78

Chapter 1

LOFAR

LOFAR (the LOW-Frequency Array, <http://www.lofar.org>) is the precursor of a new generation of radio observatories. Originally designed and built by ASTRON in the Netherlands, funded by national and regional subsidies and by a consortium of universities and research agencies, it promises a gain of two orders of magnitude in sensitivity and angular resolution over present instruments in the frequency range of 30 to 240 MHz. LOFAR is now open to collaborations in Europe, with two main goals: extending the baselines to reach an arcsecond resolution, and broadening the scientific base necessary to obtain the best return from this instrument, which addresses important questions in very different fields of astrophysics, from the early ages of the Universe to the formation of new stars and planets, and to the most violent and energetic phenomena observed in the environment of galaxy clusters, accreting black holes and in cosmic explosions. The sensors for radio astronomy are simple and fixed, organized in stations of up to 96 low-frequency dipoles and 96 tiles of 16 high-frequency antennae. Originally LOFAR was designed to be a 77 stations spread across the Netherlands (< 100 km baselines). After a recent 'de-scope' of the project, only 40 dutch stations are now envisaged, plus a number of international stations (extended LOFAR, E-LOFAR). Already involved countries in building international LOFAR stations are Germany (5 stations), UK (1 station), Sweden (1 station) and France (1 station). Italy, Poland, Ukraine, Austria and Ireland are interested to join and are seeking the needed funding, while other countries are currently discussing their possible participation. For the E-LOFAR 40 Dutch stations plus other 40 international stations, with baselines

up to 500-1000 km and optimised uv coverage, are hopefully envisaged. This Europe-wide extension is currently funded by institutes or national grants, and the establishment of a formal European consortium is under way. Still open to the participation of more European countries, it will allow scientists from these countries to join the existing collaborations ("Key Science Projects") or to propose new ones. Two firsts very successful European workshops 'Astrophysics in the LOFAR area' and Astrophysics with E-LOFAR took place in April 2007 and in September 2008, respectively. The design of LOFAR rests on recent progress in long-wavelength radioastronomy, such as RFI mitigation (dealing with RF signals, mostly of human origin), accommodation of ionospheric perturbations, and digital electronics: this leads to the concept of a complex array of a large (about 15000) number of (relatively) simple sensors, where most of the complexity resides in the digital electronics and embedded software. For centralized filtering and correlation LOFAR uses a supercomputer (IBM Blue Gene, equivalent to the largest computer available for public research in Europe), in addition smaller clusters of computers in different European sites are also planned to help in the correlation of a subset of LOFAR experiments. The digital nature of most of the processing makes it possible to synthesize as many as four independent beams that permit simultaneous observations in multiple directions. Independent programs of research, development or outreach can thus each benefit from using the array at both full resolution and sensitivity. A unique capability is to perform a posteriori pointings, in response to alerts from internal or external origin. LOFAR is thus the first of a new generation of instruments, culminating with the Square Kilometer Array which will extend to higher frequencies with a much larger collecting area in about 2020.

Chapter 2

Cosmology with LOFAR

2.1 The Cosmic Dark Ages and Reionization

Although observations of cosmic epochs closer to the present has indisputably shown that the cosmic gas is a (re-)ionized state, it is yet unclear when the phase transition from the neutral state resulting from the recombination process (occurred 300,000 years after the Big Bang) to the ionized state started. This is partly because of the uncertainties related to the sources responsible for the production of ionizing photons: stars, quasars, dark matter particle annihilation/decays, virialized gas inside cosmic structures are the most plausible guesses. Even more puzzling is the fact that for each of these sources a plethora of different possibilities exists (metal-free or normal stars? Quasars or mini-quasars? What type of dark matter particles and hence produced radiation spectra? Gas in galaxy halos or groups?). The next problem to be solved is the determination of the history of reionization towards its completion. This evolution is governed by a complex network of interlinked physical processes (in brief: feedback): the ultraviolet radiation (and the associated heavy element production by stars) necessary to reionize the cosmic plasma affects galaxy and star formation, possibly depressing it. In this case one expects a delay in the reionization progress. The post-reionization Universe is also filled with precious information on how reionization proceeded and on the sources that caused it. In fact, leftovers of reionization as neutral hydrogen islands that could not be completely turned into ionized patches are routinely detected by absorption line experiments targeting distant quasars. Even our courtyard, the halo of the

Milky Way, can be populated by the most ancient (and perhaps first) stars in the Universe, surviving as cosmic fossils. Their study can open unexpected new windows on the understanding of reionization and the fascinating epoch at which the first cosmic light was produced. The entire field will witness an even stronger burst of experimental activity in the next years. Following the PLANCK satellite, which will allow to obtain improved measurements of the CMB temperature and polarization spectra, interferometers like ALMA and ACT will explore for the first time the sub-arcminute features of the secondary anisotropies spectrum resulting, among other processes, from patchy reionization. If searches for high- z quasars and GRBs which can then be used as targets for absorption line experiments (to be carried on with VLT and ELT) will prove successful, it will be possible to investigate the reionization evolution in exquisite detail. Theoretically, to improve cosmic reionization modelling, the key issues are essentially three: (a) Simulate larger cosmic volumes in order for them to be representative of the entire cosmic reionization process; (b) Improve radiative transfer treatments to take care of the effects of small scales gas/radiation inhomogeneities and anisotropies; (c) include at best the effects of the different feedback types (radiative, mechanical, chemical - see below). Also, it will be important to improve limits on the nature of the reionization sources. This has obviously to be a joined effort of observations AND theory, but the latter can help in predicting number counts, luminosity functions, supernova/GRB rates associated with different (black hole-powered, stellar and other) source types. Particularly important is the fact that reionization could provide one of the most solid ways to to constrain the nature of dark matter, if the latter is constituted by decaying/annihilating particle, thus complementing analogous more local studies that will be carried on by GLAST.

2.2 The Cosmic Dark Ages at 21 cm

It has long been known (e.g. Field 1959) that neutral hydrogen in the IGM and gravitationally collapsed systems may be directly detectable in emission or absorption against the CMB at the frequency corresponding to the redshifted HI 21 cm line (associated with the spin-flip transition from the triplet to the singlet

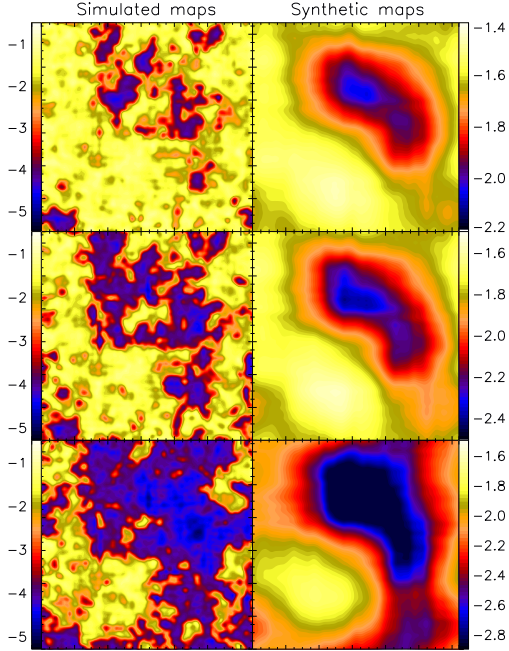


Figure 2.1: Logarithmic brightness temperature, $\log[\delta T_b/K]$, maps (linear size ≈ 10 arcmin) of the 21 cm emission for the late reionization model S5 at redshifts $z = 10.6, 9.89, 9.26$ from top to bottom, respectively. Left panels: maps obtained directly from the simulation, i.e. before convolution with LOFAR characteristics; Right: LOFAR synthetic maps. Taken from Valdes et al. 2006, MNRAS, 369, 66).

ground state). Madau, Meiksin, & Rees (1997) first showed that 21 cm tomography could provide a direct probe of the era of cosmological reionization and reheating. In general, 21 cm spectral features will display angular structure as well as structure in redshift space due to inhomogeneities in the gas density field, hydrogen ionized fraction, and spin temperature. Several different signatures have been investigated in the recent literature: *(i)* fluctuations in the 21 cm line emission induced by the “cosmic web” (Tozzi et al. 2000), by the neutral hydrogen surviving reionization (Ciardi & Madau 2003; Furlanetto, Sokasian & Hernquist 2004; Zaldarriaga, Furlanetto & Hernquist 2004; Furlanetto, Zaldarriaga & Hernquist 2004b; He et al. 2004; Mellema et al. 2006b), and by minihalos with virial temperatures below 10^4 K (Iliev et al. 2002, 2003); *(ii)* a global feature (“reionization step”) in the continuum spectrum of the radio sky that may mark the abrupt overlapping phase of individual intergalactic HII regions (Shaver et al. 1999); *(iii)* and the 21 cm narrow lines generated in absorption against very high-redshift radio sources by the neutral IGM (Carilli, Gnedin, & Owen 2002) and by intervening minihalos and protogalactic disks (Furlanetto & Loeb 2002). While an absorption signal would be

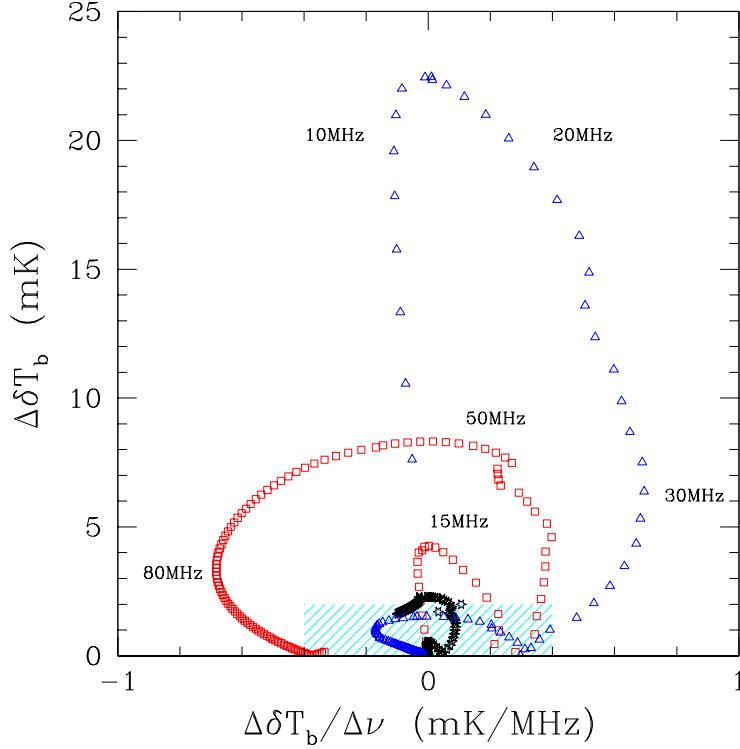


Figure 2.2: Deviations of the differential brightness temperature (y-axis) and its gradient (x-axis) from those predicted in the standard case (taken from Valdes et al. 2007, MNRAS, 377, 245). The diagram illustrates the capability of constraining DM with future 21 cm observations. The black stars, red squares and blue triangles represent 25-keV decaying WDM, 10-MeV decaying LDM and 10-MeV annihilating LDM, respectively. The shaded area indicates the parameter space in which detection is excluded given the expected observational capabilities. Numbers along the curves refer to frequencies in MHz units. hardly successful observations.

preferable, being of a higher intensity, it relies on the existence of powerful radio sources at high redshift, which have not yet been found. A possibility would be the radio afterglow of GRBs or hypernovae (which could in principle be visible up to $z \sim 20 - 30$), but the estimated absorption lines are very difficult to detect also with the next generation of radio telescopes (Ioka & Meszaros 2004). On the other hand, a signal in emission, although weaker than the one in absorption, would always be present, as long as the IGM is not completely ionized.

An exciting possibility offered by a detection of the 21 cm (1420 MHz) signal from the Dark Ages is to determine the presence of the annihilating/decaying dark matter radiation. At very high redshift ($z \sim 50 - 100$) the spin temperature of the HI, T_s , is locked to the kinetic temperature of the gas, T_k , as long as the collisional excitation

rate of the hyperfine structure is sufficiently high. As T_k is lower than the CMB temperature, due to the adiabatic cooling produced by Hubble expansion, this results in a 21 cm absorption signal at frequencies corresponding to $1420 \text{ MHz}/(1+z) \sim 20\text{--}30 \text{ MHz}$. The presence and amplitude of such feature is an undisputed signature of the linear evolution of the density field. However, DM-produced radiation could erase/modify this feature due to the corresponding (i) increase of T_k , (ii) change in the HI ionization fraction, (iii) Ly α pumping of the spin temperature. Although quite challenging (it would be carried out at best by radio-telescopes based on the dark side of the Moon to get rid of the ionospheric noise), a measure of this effect would provide one of the most clear indications on the nature of the dark matter particles. HI 21 cm data could also constrain the size of ionized (H II) bubbles around sources (typically quasars) located close to the end of reionization. The detection of H II regions will provide specific sites where high-redshift galaxies and quasars must be present. The absence of neutral hydrogen within H II regions means that these are also sites where the sources can be studied with less interference from rest-frame Ly α absorption. Some of these regions will house luminous quasars, while most will host galaxies and groups of galaxies. Although in principle quite attractive, the feasibility of this method requires careful assessment and calibration against radiative transfer cosmological simulations of the H II regions around bright high-redshift quasars in large volumes.

Ciardi & Madau (2003) used numerical simulations of hydrogen reionization by stellar sources to investigate the 21 cm signal expected from the diffuse, neutral IGM. They found that the predicted brightness temperature fluctuations on arcmin scales are typically much higher than those expected from minihalos, with values in the range $5\text{--}20 \text{ mK}$ on scales below 5 arcmin. Iliev et al. (2002, 2003) find that the signal expected from minihalos is comparable to the signal from the IGM. Shapiro et al. (2006) use numerical simulations to calculate the relative importance of IGM and minihalos (in terms of brightness temperature, not its fluctuations), finding that the latter dominate the emission at $z \leq 18$, while they are negligible at higher redshifts. In their analysis though they neglect the effect of Ly α pumping and feedback, which can be crucial once the first sources of radiation start to shine. The inclusion

of such mechanisms shows that the contribution from minihalos is almost always lower than that from the diffuse IGM (Furlanetto & Oh 2006). These fluctuations can possibly be detected by the planned facilities SKA¹ (Square Kilometer Array), LOFAR² (LOw Frequency ARray), PAST³ (Primeval Structure Telescope; Pen, Wu & Peterson 2004; Peterson, Pen & Wu 2005) and MWA⁴ (Mileura Widefield Array). In particular, LOFAR will be able to detect individual HI structures at $z \sim 11$ on arcmin scales, emitting at a brightness temperature of ~ 35 mK as a $3\text{-}\sigma$ signal in about 1000 hours of observing time (Valdes et al. 2006). It is interesting to note that for most purposes non-Gaussianity in 21cm fluctuations can be ignored and the distribution can be described with Gaussian statistics. This fact might greatly help to keep foregrounds under controls as they would be primarily responsible for any non-Gaussianity feature of the signal.

The same telescopes should also be able to distinguish between different reionization models and discriminate, e.g., a history with discrete HII regions from one with partial uniform ionization or from a double reionization (Furlanetto, Zaldarriaga & Hernquist 2004b). As the expected angular resolution is sensitive to scales that correspond to the transition between ionized and neutral regions for hard ionizing photons sources, additional information on their nature could come from observations of single ionized regions (Zaroubi & Silk 2005), also in the form of spectral dips in frequency space along single lines of sight (Kohler et al 2005). This technique though would be compromised once ionized regions start to overlap.

A key physical mechanism in order to ensure a detectable 21 cm signal is the decoupling of the CMB temperature from the spin temperature, as the latter regulates the 21 cm line absorption/emission. It has been shown (Chuzhoy & Shapiro 2006) that the exact value of the spin temperature depends on physical processes usually are not included in the calculations, the most important being the backreaction of resonant scattering on the pumping radiation and the scattering by resonant photons other than Ly α (the latter though does not affect the 21 cm line

¹<http://www.skatelescope.org>

²<http://www.lofar.org>

³<http://astrophysics.phys.cmu.edu/~jbp>

⁴<http://web.haystack.mit.edu/arrays/MWA/>

emission/absorption theory, but other lines, such as the D one). In addition, it is usually assumed that the spin temperature is decoupled from the CMB temperature due to scattering with Ly- α photons (the Wouthuysen-Field effect; Wouthuysen 1952; Field 1958) but its strength can be overestimated if a proper treatment of the Lyman series cascades is not included (Hirata 2006; Pritchard & Furlanetto 2006a). This though affect the 21cm signal only during a narrow range of redshift near the beginning of reionization, as a later times there are so many UV photons that these corrections are minor. Moreover, before a Ly α background is established, the bias in the galaxy distribution can induce fluctuations in the Ly α , and thus 21 cm, flux (Chen & Miralda-Escudé 2006). These could be used to probe the distribution of the very first galaxies (Barkana & Loeb 2005b, Wyithe & Loeb (2007). Kuhlen, Madau & Montgomery (2006) use hydrodynamic simulations of structure formation to study the effect of X-rays on 21cm line. They have a resolution in dark matter of 2000 M_{\odot} . In a simulation without sources they find that, while regions with $\delta \leq 1$ decoupling is not effective, for higher density contrasts H-H collisions are efficient at decoupling and most of the gas is shock heated, producing a signal in emission. When the effect of mini-quasars is included, the X-ray radiation preheats the IGM to a few thousand kelvins and the increased electron fraction boosts both the H-H and the H-e collisions (see also Nusser 2005a for the efficiency of H-e collisions in the decoupling during the very early stages of reionization). Thus also low density regions in the IGM can be seen in emission. It should be noted though that, although X-ray are usually considered to uniformly penetrate the IGM, this is not true at all times and might affect the 21 cm line signature (Pritchard & Furlanetto 2006b).

Also the mechanism that can heat the gas above the CMB temperature is crucial for the observation of the line in emission. In addition to Ly- α and X-ray photons (e.g. Madau, Meiksin & Rees 1997; Chen & Miralda-Escudé 2004), also UHECRs and decaying dark matter particles can heat the gas (Shchekinov & Vasiliev 2006). But it's been shown that Ly- α scattering is not an efficient mechanism to heat the IGM (Chen & Miralda-Escudé 2004; Chuzhoy & Shapiro 2006; Furlanetto & Pritchard 2006a), while X-rays are better, although they can uniformly heat the IGM only after sometime after the first structure formation (Pritchard & Furlanetto

2006b; Zaroubi et al. 2006).

Another signal detectable in the 21 cm radiation is its polarization. Although intrinsically unpolarized, in the presence of a magnetic field, the 21 cm line would show a left- and right-handed polarized component due to the Zeeman effect (Cooray & Furlanetto 2005). In addition, also scattering between electrons produced during reionization and the 21 cm quadrupole would induce polarization (Babich & Loeb 2005). Such observations would probe the magnetic field on scale of HII regions around bright quasars or the intergalactic magnetic fields. An alternative method to probe such magnetic fields would be through the imprint they leave on the brightness temperature fluctuations (Tashiro & Sugiyama 2006b).

However, this experiment is extremely challenging due to foreground contamination from unresolved extragalactic radio sources (e.g. Di Matteo et al. 2002), free-free emission from the same reionizing halos (e.g. Oh & Mack 2003), synchrotron emission from cluster radio halos and relics (Di Matteo, Ciardi & Miniati 2004) and the Galactic free-free and synchrotron emission (Shaver et al. 1999). As the foregrounds are slowly varying as a function of frequency, it appears that the best strategy for measuring the 21 cm signal would be to search for frequency rather than angular fluctuations (Di Matteo et al. 2002; Gnedin & Shaver 2004; Zaldarriaga, Furlanetto & Hernquist 2004; Santos, Cooray & Knox 2005; Wang et al. 2006). Di Matteo, Ciardi & Miniati (2004) have used cosmological simulations to predict the impact of extragalactic foreground produced by both extended (e.g. cluster radio halos and relics) and point-like (e.g. radio galaxies and free-free emission from ISM) sources. They find that the contribution to the angular fluctuations at scales $\theta \geq 1$ arcmin is dominated by the spatial clustering of bright sources. Hence, efficient removal of such sources may be sufficient to allow the detection of angular fluctuations in the 21 cm emission free of extragalactic foregrounds.

Finally, we note that low frequency radio observation might be able to detect the signal associated with the cosmological deuterium. Before UV radiation is emitted, the ratio between the emissivities from D (91.6 cm) and H (21.1 cm) hyperfine transitions is proportional to D/H. Thus a cross correlation between the two lines can be used to derive precise estimates of the primordial abundance of D (Sigurdson

& Furlanetto 2006). Due to the different collisional cross-sections (D-H against H-H), T_S^D can be decoupled from T_{CMB} down to $z \sim 1$ and in principle be observed in absorption also at low redshift. Once Ly photons are produced, in addition to collisions, scattering becomes a primary process for the decoupling. In this case though the ratio between the two radio emissions would not be proportional to D/H anymore (Chuzhoy & Shapiro 2006). In fact, T_S is affected by scattering with Ly photons (although the decoupling become less efficient with time due to the back reaction of the scattering process onto the photon spectrum). While T_S^H is unchanged by the inclusions of higher Ly orders, T_S^D is heavily affected by Ly β photons. This means that the ratio of the two lines after UV photon production depends on the spectrum and is no more directly proportional to D/H. In addition, T_S^D can become negative and the line can be seen in emission also if $T_k < T_{CMB}$.

2.3 21 cm temperature fluctuations and the structure formation

As already pointed out in the previous sections, the reionization history is strictly dependent on the UV source distribution. In order to describe this quite complex scenario, many analytic, semi-analytic and numerical models proposed up to now (Gnedin 2000, Ciardi et al. 2003b, Wyithe & Loeb 2003, Barkana & Loeb 2004, Haiman & Holder 2003, Madau et al. 2004, Wyithe & Cen 2007, Choudhury & Ferrara 2007, Iliev et al. 2007, Ricotti et al. 2008) relate the statistical properties of the ionized regions and the ionizing galaxies, making assumptions for the ionization and the recombination processes acting on the IGM. Assuming a hierarchic formation of the structures, the first sources of light form at high redshift in the highest peaks of dark matter, consequently the reionization process is affected by the cosmological environment and depends on the power spectrum of the primordial overdensity field.

For instance, the possible presence of a dark energy component can affect the statistical distribution of the ionized regions with repercussions on the amount of ionized IGM (filling factor) at the different cosmological epochs and, as a consequence, on the time-scale for the reionization end (Maio et al. 2006, Crociani

et al. 2008). The reionization picture is well described in the 'standard' Λ CDM universe, i. e. a flat universe dominated at late redshifts by a constant dark energy component characterized by a constant equation of state $p = w\rho c^2$. But although the recent observations suggest that $w \sim -1$ at late redshifts, its temporary evolution is up to now not well constrained and several observational datasets of luminosity distances for Type Ia supernovae do not reject the possibility that w depends on z . In these so-called quintessence scenarios, the main effect of $w > -1$ is an earlier growth of matter fluctuations and a higher number density of dark matter halos at the same cosmological epoch, that indeed affect the HII region distribution. Under the assumption of a given quintessence model, predictions on quantities that can be constrained by the 21 cm observations, as the ionized fraction of the IGM or the typical size of the HII regions, can be made. Through the simplest analytic approaches used to describe the ionization process of the IGM, a preliminary investigation of the distribution of the ionized bubbles allowed us to estimate the expected distribution of the radii of the HII regions, that can be a factor 2 smaller than in the 'standard' Λ CDM cosmology when the recombination process is considered. As a consequence, the IGM filling factor can rise to twice that obtained for the 'standard' cosmological scenario. We should note that these results can be affected by the simplest nature of the theoretical approach and more accurate numerical simulations are in progress to give a better picture of reionization. A preliminary investigation of the imprinting on the inhomogeneous reionization of the quintessence has been made by Pritchard, Furlanetto & Kamionkowi (2007). They showed that observations of small ionized bubbles can probe the dark energy w parameter with $\sigma_w \sim 0.4$ at late epochs.

On the other hand, also the nature of the primordial density field is expected to have effects on the reionization epoch. Although the 'standard' inflation scenario produces an almost adiabatic and Gaussian-distributed density field, the last investigations of the CMB spectrum and the distribution of quasars in the Sloan Digital Sky Survey suggest that small deviations from primordial Gaussianity are allowed. This should affect the distribution of the highest peaks in which the galaxies form and as a consequence the morphology of the ionized regions. However we have

to note that the exact nature of the primordial non-Gaussianity, and in particular its possible dependence on the physical scale, is still debated. Several works (e. g. Crociani et al. 2008, Cooray et al. 2008, Avelino & Liddle 2006, Chen et al. 2003) discuss the possibility of constraining the primordial non-Gaussianity through measurements of the reionization epoch, making predictions for the optical depth or the filling factor of the IGM, that could be estimated by the future 21 cm maps. Assuming a parameter f_{NL} (namely the amplitude of the second-order correction to a Gaussian field) to represent the level of non-Gaussianity, we obtain an enhanced formation of dark matter halos when $f_{\text{NL}} > 0$. This indeed produces a higher collapsed fraction than that predicted in a standard Λ CDM universe ($f_{\text{NL}} = 0$) at the same epoch and as a consequence the filling factor could be a factor 10 higher, when extremes non-Gaussianity parameters are considered. However, the effect on the IGM optical depth is smaller than 10 per cent and an accuracy higher than that of present CMB-like experiments is needed to probe the nature of non-Gaussianity. These results, which need to be confirmed by numerical simulations, are supporting the crucial role of LOFAR to probe not only the reionization epoch but also for a deeper investigation of the structure formation scenario.

2.4 Alcock-Paczyński test at high redshift with the 21cm line

The 21 cm emission from the reionization epoch contains information pertaining to cosmological parameters such as the expansion history of the universe and the growth of density fluctuation that, together, can shed light on the nature of the dark energy and constrain alternative theories of modified gravity theories (Guzzo et al. 2008 Nature 451 541 , Linder E., 2008 Astroparticle Physics 29 336, Wang Y., 2008 JCAP 05 021).

Provided that one can successfully handle the overlying astrophysics, LOFAR could allow to map the 3D structure of the redshifted 21 cm signal. It is well known that the correlation analysis of such a signal, either in real or in Fourier space allows, in principle, to constrain all relevant cosmological parameters (e.g. McQuinn et al. 2006, ApJ, 653. 815). When analyzing these maps, however, one has to bear in

mind that the signal is measured in redshift rather than in real space since the 21 cm brightness temperature is specified along a given direction and a frequency, or redshift. Peculiar velocities spoil the one-to-one correspondence between proper distances and redshifts and systematically modify the auto-correlation properties of the signal. Moreover, since the correlation is measured between pixel maps at given angular separations, adopting the wrong cosmological model induces an additional distortion known as Alcock-Paczyński effect (1979, *Nature*, 281, 358). The possibility of detecting the Alcock-Paczyński distortion in the redshifted 21-cm maps has first been examined by A. Nusser (2005, *MNRAS*, 364 743).

Here we propose to detect and analyze the full distortion pattern to extract all available cosmological information. The idea is illustrated in Figure 2.3 which shows the expected iso-correlation contours of the 2-point spatial auto-correlation function of the 21 cm signal emitted at a reionization epoch of $z = 8$ and measured in redshift space, $\xi(r_p, \pi)$. The correlation in the 3D emission maps is measured between pairs with a transverse separation Δr_p (X-axis) and radial separation $\Delta \pi$. In absence of distortion effects the color-coded iso-correlation contours would be circular. Peculiar velocities introduce distortions along π that can be naturally separated in two components. A small scale pairwise velocity dispersion responsible for the elongation of the contours at small values of r_p and that are likely to be obliterated by the intrinsic correlation of the reionization pattern, and coherent bulk motions at large separations responsible for the compression of the iso-density contours at high values of r_p . This second type of distortion is less sensitive to the details of the reionization and can be used to estimate the growth rate of density fluctuation which, in Einstein's gravity theory, is simply $f(\omega_m) \simeq \Omega_m^{0.55}$, with Ω_m representing the luminous+dark mass density parameter. Deviations from this simple relation would be the signature of modified gravity. The Alcock-Paczyński effect represents the third type of distortions which is introduced by relating the measured angular separation $\Delta \theta$ to r_p through $r_p = \Delta \theta H(z) D_A(z)$. In this relation both the expansion history, $H(z)$, and the angular diameter-redshift relation, $D_A(z)$, depend on the fundamental cosmological parameters. Assuming an incorrect cosmological model induces an additional distortion in the correlation

pattern which can also be detected at large separations. The distortion patterns induced by the three effects can be easily modeled and separated from each other, provided that the signal-to-noise of the auto-correlation signal at large separation is high enough.

Therefore, comparing model predictions with the auto-correlation signal of the 21 cm brightness temperature map observed by LOFAR not only allows to estimate the fundamental cosmological parameters (through the Alcock-Paczyński test) but also provide a check to break the degeneracy between Dark Energy models and theories of modified gravity.

2.5 Structure formation at high redshift in non standard cosmological scenarios

We outline in this Section two possible scientific cases that could be addressed by LOFAR: *i*) mapping the dark energy component from low to high redshifts with a particular focus on its equation-of-state $p = w \rho$; *ii*) tightening some constraints on the linear dark matter power spectrum $P(k)$ and the growth factors of density perturbations. Even if the present state-of-the-art picture in terms of cosmological parameters seems robust and concordant towards a Λ CDM model there are still inconsistencies and tensions between some cosmological parameters as derived from different data sets, such as the values of σ_8 , Ω_m , the presence of a running spectral index and the behaviour of $P(k)$ at small scales (e.g. Komatsu et al. 2008 arXiv:0803.0547, Lesgourgues et al.2007, JCAP, 11, 008).

Assuming that the main astrophysical uncertainties will be treated properly and constrained by LOFAR or other similar experiments it is possible to study some statistical properties of the density field at high redshift. However, what is actually observed is the 21 cm brightness temperature relative to the CMB at a position \mathbf{x} and its fluctuations over the mean: $\delta(\mathbf{x}) = (\delta T_b(\mathbf{x}) - \delta T_b / \delta T_b)$. If we expand to linear order the above quantity the different contributions can be disentangled and $\delta \sim \beta_b \delta_b + \beta_X \delta_X + \beta_\alpha \delta_\alpha + \beta_T \delta_T - \delta^{pecvel}$, where the δ terms indicate fractional variations in the baryonic density, the neutral fraction, the Lyman- α coupling coefficient, the gas kinetic temperature and the line-of-sight

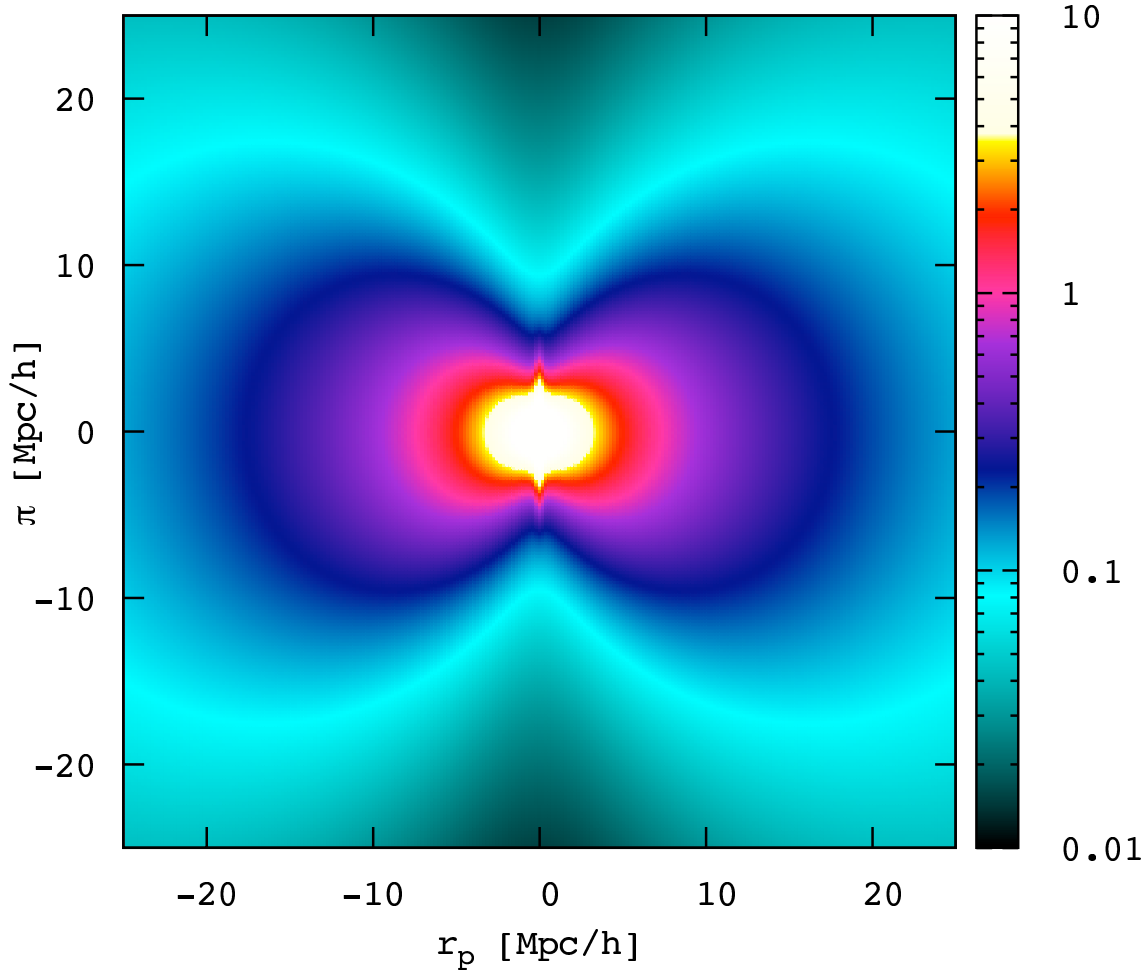


Figure 2.3: Estimate of the degree of distortions introduced by Alcock-Paczyński effect and peculiar motions on the measured 21 cm brightness temperature map from the reionization epoch. The color scale represent the iso-correlation contour of $\xi(r_p, \pi)$, measured at $z \sim 8$ as a function of the transverse r_p and radial π separation of map element pairs. The measurement is replicated over four quadrants to show deviations from circular symmetry. Peculiar velocity combine with geometrical effect derived from having assumed the incorrect cosmological model ($\Omega_m = 0.25, \Omega_\Lambda = 0.75$ in the case shown), producing the distorted pattern when the redshift is used as a distance measure.

peculiar velocity gradient (see Furlanetto, Oh & Briggs 2006). The behaviour of each coefficient strongly depends not only on the cosmological model but on the reionization history of the universe and many astrophysical parameters. All these contributions apart from the peculiar velocities are isotropic and can be collected into one single term in Fourier space in such a way $\delta = \mu^2 f \delta + \delta^{iso}$ (here δ indicates

the corresponding Fourier component), with μ the cosine of the angle between \mathbf{k} and the line-of-sight and $f = d \ln D / d \ln a$, with D the linear growth factor of density perturbations and a the scale factor. Linear theory can be used to relate easily (at the largest scales) the peculiar velocity contribution and that of the density via the well known equation $\delta_{pecvel} = -\mu^2 f \delta_b$. The relation above is fundamental since the power spectrum of δ is: $P(\mathbf{k}) = \mu^4 P_{\delta_b \delta_b} + 2\mu^2 P_{\delta_{iso} \delta_b} + P_{\delta_{iso} \delta_{iso}}$; the power is thereby significantly boosted thanks to the peculiar velocities and the contribution from baryonic density fluctuations can be isolated. At scales larger than the Jeans length and especially at high redshift where structures are more linear it is expected that the baryons trace faithfully the underlying dark matter density field ($\delta_b = \delta_{DM}$).

Thereby, if astrophysical parameters are known or constrained, an estimate of the dark matter power spectrum will be possible. This will open up the possibility to constrain cosmological parameters such as the dark energy equation of state: if we assume that the growth factors at $z = 0$ will be constrained with measurements of the value of σ_8 . To illustrate this issue further, we plot in Figure 2.4 the behaviour of the growth factors (normalized at the present time) as a function of the scale factor in two different cosmologies a Λ CDM universe and a SUGRA model which is well mimicked by an equation of state $w(z) = w_0 + w_a(1 + z)$ with $w_0 = -0.82$ and $w_a = 0.56$ (left panel). Models with a positive w_a are expected to show large differences in the evolution of the growth factors compared to Λ CDM. The effects on structure formation of such an evolution for the dark energy component show that the non linearity is reached earlier compared to Λ CDM. In the right panel of the same figure 2.4 we show the 1 and 2σ constraints in the $w_0 - w_a$ plane once the growth factors above are measured at $z = 8, 12, 16, 20$ with a precision of 20%. Note that in this case we assumed spatial flatness and strong priors on $H_0 = 72 \pm 3$ km/s/Mpc and Ω_m known with a 3% error. Even if these assumptions are very optimistic now they will not be unrealistic after the PLANCK measurement of CMB anisotropies. One can easily see that such an experiment will offer the possibility to distinguish between the two models, thereby between evolving dark energy and a cosmological constant, at very high significance, if such a measurement could be performed.

Another example of the different evolution of density perturbations is shown in

Figure 2.5 where the brightness temperature extracted from three different high resolution hydrodynamical simulations (30 comoving Mpc/h and 2×400^3 gas and dark matter particles) is shown at $z = 12$. In converting from the gas density field to brightness temperature, reasonable assumptions in terms of reionization history have been made: this is equivalent to assume that the reionization history is known from another set of independent observations. Three different curves are shown here: two Λ CDM models with very different recipes for the feedback and for the star formation criterion (blue and red curves) and a dark energy (DE) model which is very different from the standard cold dark matter case and resembles the modified gravity models of Tsujikawa (2008, PhysRevD, 77, 023507). The most important things are: *i*) astrophysical galactic or sub-galactic processes do not modify the probability distribution function and the overall properties of the cosmic web; *ii*) the DE model is different, especially in the low brightness tail from the standard one. We have to stress that in order to be sensitive to such small differences in the temperature brightness probability distribution function a high spatial resolution (sub-Mpc scale) is demanding making the case for an extended LOFAR array very important.

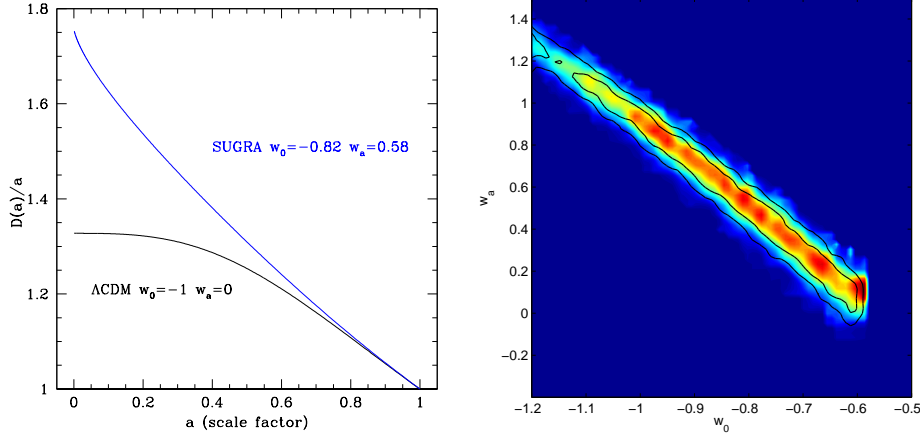


Figure 2.4: Left: Evolution of the growth factor as a function of the scale factor for two different cosmological models a Λ CDM model with $w = -1$, and a SUGRA model can be mimicked by the shown values for the dark energy equation of state, which is parametrized by $w(z) = w_0 + w_a(1 + z)$. Right: 1 and 2σ constraints achievable for the equation of state from an hypothetical experiment able to measure the linear growth factors of figure 1 with a precision of 20% at $z = 8, 12, 16, 20$. The fill (empty) contour represent the mean (marginalized) likelihood.

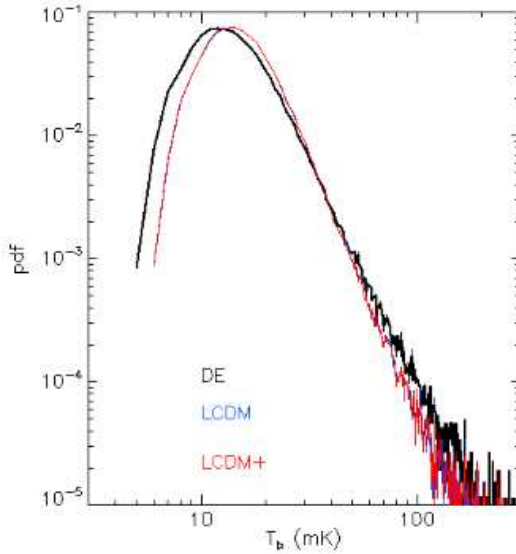


Figure 2.5: Probability distribution function of the observed brightness temperature in mK as extracted from three different hydrodynamical cosmological simulations at $z = 12$. The LCDM lines in blue and red indicates the standard scenario with two very different criteria for star formation and feedback, while the DE model in black refers to a simulation with a dark energy component that follows the model proposed by Tsujikawa (2008, PhysRevD, 77, 023507).

Chapter 3

Extragalactic Surveys

3.1 Survey plans

An important goal that has driven the development of LOFAR since its inception is to explore the low-frequency radio sky by means of a series of unique surveys. The current plan is to exploit the unprecedented sensitivity and wide instantaneous field of LOFAR to conduct large-sky surveys at 15, 30, 60, 120 and 200 MHz. Such surveys should start in 2009, when the 100 km LOFAR should become operational. In the original plan (see Table 1) the surveys were designed to reach confusion limit at 15, 30, 120, 200 MHz and will be carried out over several epochs, enabling variable sources to be recognised. International baselines will increase resolution and lower the confusion limit (see Table 2 for E-LOFAR parameters at 240 MHz), so surveys are being modified. As an example, the 240 MHz survey will likely be re-scoped as follows: a) 1000 deg² to $S_{lim} = 210; \mu\text{Jy}$; b) 80 deg² to $S_{lim} = 54; \mu\text{Jy}$; c) 3 deg² to confusion limit.

3.2 Scientific Perspective of LOFAR Extragalactic surveys

Low frequency deep all-sky surveys as the ones planned with LOFAR will provide unique (both in size and in frequency coverage) catalogues of radio sources (mainly steep-spectrum star-forming galaxies and radio emitting AGNs), for investigating several fundamental areas of astrophysics, including the formation of massive black holes, galaxies and clusters of galaxies. Such catalogues will be ideal to build statistical samples of rare classes of steep and ultra-steep radio sources, like,

Table 3.1: Original survey design (for 77-station Dutch LOFAR)

Freq. (MHz)	Angular resol. (")	Sky cover	3σ S_{lim} (mJy)	Source density (arcmin ⁻²)	Source No
15	50.3	2π sr	4.7	0.2	1.3×10^7
30	25.2	2π sr	1.0	0.7	5.4×10^7
60	12.6	2π sr	1.0	0.3	2.2×10^7
120	6.3	2π sr	0.043	11.6	8.6×10^8
200	3.8	250 deg ²	0.014	32.2	3.0×10^7

Table 3.2: Relevant parameters for E-LOFAR at 240 MHz

Max. baseline (km)	Angular resol. (")	3σ confusion limit (μ Jy)
100	3.1	13
500	0.6	5
1000	0.3	1

for instance, very high redshift ($z \sim 6$) radio galaxies, cluster haloes, dying radio sources, giant radio galaxies, etc). Because the LOFAR surveys will probe unexplored parameter space, it is likely that they will discover new phenomena.

Four topics are driving the definition of the proposed surveys. These are:

- Formation of massive galaxies, clusters and black holes using $z \lesssim 6$ radio galaxies as probes,
- Intercluster magnetic fields using diffuse radio emission in galaxy clusters as probes,
- Star formation processes in the early Universe using starburst galaxies as probes, and
- Exploration of new parameter space for serendipitous discovery.

3.3 Deep LOFAR Fields and the Benefits of International Baselines

Multi-wavelength studies of deep radio fields show that the sub-mJy population, responsible for the steepening of the 1.4 GHz source counts (Condon 1984, ApJ, 287,

461; Windhorst et al. 1990, ASP Conf. Ser., 10, 389), has a composite nature. Star-forming galaxies dominate at microJy (μJy) levels (see e.g. Richards et al. 1999, ApJ, 526, L73), while radio sources associated to early-type galaxies, and plausibly triggered by AGNs, are the dominant component at flux densities $> 0.1 - 0.2$ mJy (Gruppioni et al. 1999; Georgakakis et al. 1999; Magliocchetti et al. 2000; Prandoni et al. 2001; Afonso et al. 2006; Mignano et al. 2008).

Because of the large fields of view (the primary beam per station is 1.5 deg^2 at 240 MHz), deep surveys at the highest LOFAR frequencies, able to reach μJy fluxes, will detect unprecedented numbers of star-forming galaxies up to high redshifts, already at the 100-km LOFAR confusion limit (see Table 1).

On the other hand, the benefits of using an extended LOFAR (500-1000 km baselines) is very clear for deep fields. Improving the angular resolution does lower the confusion limit and allows to fully exploit the instrument capabilities, by reaching its sensitivity limit. As an example, a 1000-km E-LOFAR would allow us to reach a flux limit of $1 \mu\text{Jy}$. At such flux limits we can detect star-forming galaxies with star formation rates of $\sim 10 M_{\text{Sun}}/\text{yr}$ at the epoch at which the bulk of galaxy formation is believed to occur ($2 < z < 3$) and with star formation rates of $\sim 100 M_{\text{Sun}}/\text{yr}$ at $z \gg 4$ (see Fig. 1).

Such deep LOFAR observations, in synergy with deep observations undertaken at different wavelengths with other present and future facilities (such as the Hubble Space Telescope, the Spitzer and Herschel satellites, the SCUBA-2 sub-mm imaging array and the ALMA (sub)-mm interferometer, the Chandra and XMM satellites, etc., SEE SECTION FIORE), will give a full understanding of the nature and evolution of star-forming galaxies at high redshifts and thus facilitate a census of the cosmic star-formation history, unhindered by the effects of dust obscuration.

3.3.1 The AGN component

The somehow unexpected presence of large numbers of AGN-related sources at sub-mJy fluxes has given another interesting scientific perspective to the study of deep radio fields, since a better understanding of the physical and evolutionary properties of such low/intermediate power AGNs may have important implications on the

determination of the black-hole-accretion history of the Universe as derived from radio-selected samples; and, more generally, would allow us a better understanding of the triggering mechanisms of AGN radio activity.

Of particular interest is the possibility of assessing whether the AGN component of the sub-mJy population is more related to efficiently accreting systems - like radio-intermediate/quiet quasars - or to systems with very low accretion rates - like e.g. jet-dominated FRI (Fanaroff & Riley 1974, MNRAS, 167, 31) radio galaxies. The latter scenario is supported by the presence of many optically inactive early type galaxies among the sub-mJy radio sources, whereas the *quasar* scenario may be supported by the large number of so-called radio-intermediate quasars found at mJy levels (see e.g. Lacy et al. 2001, ApJ, 551, L17). In addition, Jarvis & Rawlings (2004, New Astron. Rev., 48, 1173) tried to model the contribution of radio-quiet AGNs at faint radio fluxes (by converting the hard X-ray luminosity function into a radio LF), and propose a scenario in which radio-quiet quasars strongly affect the radio counts in the flux range 0.3 – 1 mJy. Another issue is represented by the role played at low radio fluxes by low radiation efficiency accretion mechanisms, associated to optically thin disks, such as the so-called advection dominated accretion flows (ADAF) and modifications (ADIOS, CDAF etc.; see Narayan & Yi 1994, ApJ, 428, L13; Quataert & Narayan 1999, ApJ, 520, 298; Abramowicz et al. 2002, ApJ, 565, 1101).

Very useful information may come from the study of both the radio morphology and the radio spectral properties of the faint radio population, since different triggering mechanisms (e.g. star-formation vs nuclear activity) and different accreting regimes in AGNs display different morphology and spectral signatures in the radio domain. However, the study of nuclear activity in deep radio fields has been recognized as promising only very recently, and multi-frequency radio data - typically 1.4 GHz observations followed-up at 5 or 8.4 GHz - are available only for a very limited number of sub-mJy samples.

LOFAR gives the possibility of getting multi-frequency information in a domain very poorly explored at mJy and sub-mJy fluxes (the few available low frequency follow-ups of deep fields mainly come from 610 MHz observations with the GMRT).

To conclude it is worth mentioning that a clear understanding of the nature and evolutionary properties of the various components of the sub-mJy population with LOFAR and other upcoming SKA pathfinders is of critical importance for providing reliable modeling of the nanoJy radio sky which will be eventually probed by the SKA itself.

3.3.2 The starburst galaxies component

The other major contribution to the sub-mJy radio population comes from starburst galaxies.

Constraining the star formation history and stellar mass evolution of galaxies is a central component of understanding galaxy formation. Observations of the stellar mass and star formation rate density at both low and high redshifts indicate that most of the activity responsible for shaping the bulk properties of galaxies to their present form occurred in the epochs between $z \sim 1$ and $z \sim 3$. Therefore derivation of the star formation rate for a large number of galaxies in this crucial redshift range, is of the highest importance.

Comparison between the observed star formation density evolution and the prediction of semianalytical models of star formation can also place constraints on the models. At present, there are large discrepancies in the sense that models tend to underestimate the observed star formation rate (e.g. Daddi et al. 2007, Santini et al. 2008). However there are still large uncertainties and biases in the derivation of the star formation rates from the observations: many indicators are used at different redshift and different wavelength ranges, including the UV continuum, UV and optical nebular emission lines, the mid-IR emission, the X-ray and the radio emission.

In this context the use of the radio flux as an indicator of SFR is extremely useful: radio emission is not affected by dust obscuration, whose variation dominates the systematic uncertainty in the SFRs derivation of many of the above indicators. However so far, the main studies have been hampered by the uncertainties in determining the exact nature of the submJy sources given their low luminosities at other wavelengths and the difficulty in discriminating between low luminosity

AGN and true SF galaxies (e.g; Seymour et al. 2008).

With its unprecedented sensitivity to non-thermal radio emission from star formation, LOFAR will detect large numbers of star-forming galaxies, precisely at the epoch where we believe that the bulk of galaxy formation occurred i.e. between $z \sim 1$ and 3. In particular, LOFAR should be able to detect a nearby normal star-forming galaxy, such as M82, out to redshift 1 and an ultra-luminous infrared galaxy, like Arp 220, out to redshift 34 (Garrett 2002).

Deep LOFAR surveys in combination with data from other facilities will therefore allow a census of the global star formation density evolution. In addition, the combination with the future far-IR and millimeter facilities such as SIRTf, ALMA, and JWST, will allow to assess the evolution of the far-IR -radio correlation (e.g. Cariulli & Yun). Combination with deep multiwavelength data from other surveys, from optical to mid-IR, will also allow a global investigation of galaxy properties, such as stellar masses, ages and specific star formation rates, and assess the contribution to the star formation density by galaxy stellar mass and other related open issues.

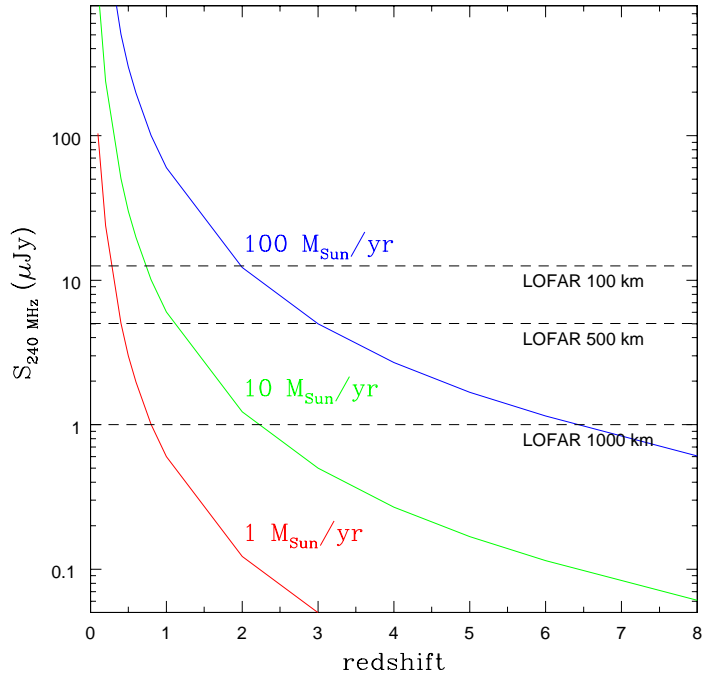


Figure 3.1: Expected flux at 240 MHz as a function of redshift and star formation rate. Dashed lines give the LOFAR sensitivity limit (confusion limit) assuming different configurations.

Chapter 4

Radio Galaxies and Quasars

4.1 Energetics & Spectrum of particles

The synchrotron radiation from extragalactic radio sources is emitted by relativistic electrons (and positrons) embedded in magnetic fields with strength in the range 1–1000 μG . The origin and evolution of these particles is an issue of great interest in modern astrophysics. Electrons with a Lorentz factor γ in a magnetic field of intensity B (in mGauss) emit via synchrotron process at a frequency $\nu = 4.2 \times 10^{-6} \gamma^2 B$ (in GHz). Present day radio telescopes typically show us what is the energy spectrum only for electrons with Lorentz factors γ upwards of $\sim 10^3$.

The spectrum of the emitting electrons in radio sources can be generally described by a power law, $F(\nu) \propto \nu^{-\alpha}$ with $\alpha \sim 0.5 - 0.7$, that would imply a corresponding spectrum of the emitting electrons $N(E) \propto E^{-\delta}$ with $\delta \geq 2$, consequently the majority of the energy of the particles is stored at low energies, at $\gamma \leq 10^3$. LOFAR will reach unprecedented sensitivities and angular resolutions at 40 – 240 MHz providing a unique opportunity to measure the spectrum of electrons at $\gamma \sim 1000$.

4.2 Relativistic Jets

Extragalactic jets are multi-band sources, with Spectral Energy Distributions (SED) extending over basically all of the electromagnetic spectrum, and reaching up to the TeV regime in some cases. Development of new instrumentation from the radio band (e-VLA, ALMA, space VLBI) to the gamma-rays (*Fermi*, MAGIC, HESS, VERITAS) is now opening a new era in the study of the physics of extragalactic

jets.

While Inverse Compton emission is the mechanism operating at the highest energies, synchrotron emission is responsible for the low frequency component. Given the steep spectral index ($\alpha > 0.5$, $S(\nu) \propto \nu^{-\alpha}$) in the optically thin jet regions, it is clear that when one goes down to the 30-200 MHz frequency range the flux density originated in jets becomes much larger than at the centimeter wavelengths typical of present day radio astronomy. Therefore, LOFAR seems a natural instrument to complement the high energy view of the jet phenomenon.

However, by going to low frequency, one is also affected by the loss in spatial resolution and the need for long baselines becomes then evident. Resolution is of the utmost importance in the study of jets, whose typical angular sizes range from several arcsecond scales down to less than one arcsecond, or even milliarcseconds, when one is interested in the jet width and the region of jet formation. Therefore, long baselines are essential for LOFAR to play a major role in this field.

4.2.1 Jet Structure

Theoretical and numerical works are proposing that jets are structured, both radially and transversely (e.g., Ghisellini et al. 2005, Rossi et al. 2008). Observational evidence of stratification is also mounting, from total intensity, spectral index, polarization and Faraday rotation images (e.g. Giroletti et al. 2004, Gabuzda 2006). In particular, transverse velocity structures can give rise to total intensity and spectral index structures, while toroidal/helical magnetic fields can account for polarization changes and rotation measures (RM) gradients.

In order to improve the quality of the observational data, it is essential to extend the frequency range over an interval as large as possible. Since matching resolutions are required for spectral index and RM studies, the data at low frequency need to be taken with baselines as long as possible. Studies of transverse structures that are currently doable only on a small number of sources (Laing et al. 2008) will become feasible for entire populations thanks to e-LOFAR.

Moreover, the well known dichotomy between FR1 and FR2 radio galaxies does not only involve the radio luminosity but also their morphology. The jet morphology

can be influenced by the medium, the accretion process, or both. Stratification and interaction with the ambient medium give rise to steep spectrum emission, best visible at low frequency. However, arcsecond resolution is needed to disentangle these structures from the emission originating in the inner spine and discuss differences between FR1 and FR2 sources.

4.2.2 Blazars

In the so-called blazar sources (Flat Spectrum Radio Quasars and BL Lac objects), the jet dominates the SED, which is known to be variable at all wavelengths. High energy satellites have discovered time variability on scales that require high Doppler beaming. On a different energy band, Intra-Day Variability at radio frequency is explained with inter-stellar scintillation but it also requires high compactness of the emitting region (e.g. Bach et al. 2006).

Acting as a large area sky monitor, LOFAR can bring important steps forward in understanding the physics of blazars. This is particularly relevant in the *Fermi* era. The Large Area Telescope (LAT) on board *Fermi* is a pair conversion telescope designed to cover the energy band from 20 MeV to greater than 300 GeV, operating in an all-sky scanning mode, providing regular γ -ray monitoring of extragalactic sources.

Given the large number of detections expected by *Fermi* (> 1000 blazars, Lott et al. 2007), it will be very demanding to pursue identification and follow up of gamma-ray sources, correlation of light curves in the radio and gamma-ray band, and the study of luminosity functions. In this framework, the gamma-ray and the blazar community will have certainly a great interest in an instrument with large field of view and great resolution and sensitivity, such as LOFAR.

4.3 Radio Hot Spots & low energy electron cut-off

Radio hot spots are regions of enhanced radio emission located at the end of the radio lobes of FR2 radio galaxies and quasars. These regions mark the ‘working surface’ of supersonic jets in which their kinetic energy is dissipated into the acceleration of relativistic particles. Being relatively isolated regions – away from the central

galaxy core – hot spots are ideal laboratories for testing the energetics and the evolution of a radio galaxies. The *diffusive shock acceleration theory* which is commonly adopted to describe particle acceleration at hot spots (e.g., Heavens & Meisenheimer 1987; Blandford & Eichler 1987) provides a viable description of the acceleration of sufficiently energetic particles, with a Larmor gyroradius larger than that of the thermal protons (which give the thickness of the shock). The physics of acceleration of relativistic electrons with a Lorentz factor $\gamma \sim 100 - 10^3$ is based on the possibility that rather poorly known mechanisms can pre-accelerate high energy electrons to energies sufficient to be diffusively advected across the shock discontinuity and then accelerated via Fermi processes (e.g., Eilek 1991; Hoshino et al. 1992). The shape of the spectrum of the electrons below $\gamma \sim 100 - 10^3$ is thus very uncertain and observations are a unique avenue to constrain present theories. An additional complications comes from the fact that relativistic shocks may play an important role in the acceleration of particles in radio sources. These shocks that develop in the jets (e.g., Ellison, Reynolds & Jones, 1990; Kirk et al. 2000; Achterberg et al. 2001). In this case the minimum energy of the accelerated particles is due to the energy gain that particles get at the first encounter with the shock $E_{min} \sim \Gamma^2$ (Vietri 1995, Achterberg et al. 2001), Γ the Lorentz factor of the shock.

4.3.1 Hot spots as ideal e-LOFAR targets

A possible detection of a low energy cut-off has been recently claimed in one of the hot spots of the nearby radio galaxy Cyg A by making use of 74 MHz, 330 MHz and higher frequency observations at the VLA (Lazio et al. 2006), other sources are not accessible to present radio telescopes that reach poor resolutions and sensitivities at lower frequencies.

The combination of sensitivity and (sub-)arcsec resolution at low radio frequencies of e-LOFAR (~ 1000 km baselines) make this radio telescope unique in this kind of studies. Hot spots have large magnetic fields, $B > 100 \mu G$, and the synchrotron radiation at ~ 100 MHz from these regions is emitted by electrons with Lorentz factors $\gamma \ll 10^3$, i.e. by those particles that are in the range of energies

of interest to address the problem of the low energy cut-off in the context of shock acceleration.

A possible complication is given by the fact that hot spots are compact sources where synchrotron-self absorption may come into play causing a flattening of the synchrotron spectrum at lower frequencies that is not due to a flattening (cut-off) in the spectrum of the emitting electrons. This gets an upper bound to the synchrotron emissivity ϵ of the hot spots, with size l , that can be studied in the optically thin regime at frequency ν_e :

$$\epsilon_{\nu_e} \leq C_\epsilon l^{-\frac{2(3+\alpha)}{7+2\alpha}} (1+z)^{\frac{9(3+\alpha)}{7+2\alpha}} \quad (4.1)$$

where C_ϵ is a constant. By assuming equipartition this actually limits the possibility to study the electron spectrum of hot spots with a given synchrotron emissivity ϵ since the energy of electrons emitting at a given frequency scales with emissivity as :

$$\gamma \propto \left(\frac{1}{\nu_e}\right)^{1/2} \epsilon_{\nu_e}^{-\frac{1}{2(3+\alpha)}} \quad (4.2)$$

4.4 Giant radio sources

The rare species of Giant Radio Galaxies (GRGs) populates the extreme end of the linear size distribution of radio galaxies, with sizes in excess of 1 Mpc. By their very nature they stretch models of double radio sources to the limit in certain realms of parameter space. By their immense sizes they have a higher probability of being in the plane of the sky. This allows studies of intrinsic source parameters with a minimal orientation bias. The lobes of GRGs are located well outside the gaseous haloes of the parent galaxy and therefore interacting directly with, and probing, any intergalactic medium (IGM). The very existence of visible hotspots at the extremities of GRGs, typically more than 500 kpc away from the host galaxies, indicates interactions with a working surface. Here, the ejecta from the AGN encounter resistance of their propagation, the IGM. The relativistic particles resident in the lobes of GRGs have to traverse large distances, thus bearing information about

large fractions of the radio galaxies' lifetimes. Since they also cross huge volumes of intergalactic space, they can also serve as diagnostic tools of the IGM which is otherwise hardly accessible via direct observations. Using equilibrium arguments between jet ram thrust or lobe pressure and the ambient medium IGM particle densities of a few 10^{-5} cm^{-3} have been found (e.g. Mack et al. 1998, Schoenmakers et al. 2000a). As GRGs are never found in rich clusters of galaxies they are believed to develop in an environment with characteristics similar to those of the non-condensed phase of the baryons (Palma et al. 2000). However, due to the very small redshift range of current samples, it has never been possible to test evolutionary models of the IGM properly using GRGs (Subrahmanyan & Saripalli 1993). Ideally, to test the expected evolution of the IGM density of $(1+z)^5$, a sample of GRGs spanning a larger range in redshifts out to at least 1 or 2 is needed. Only very few GRGs at redshifts > 0.5 are currently known (Cotter et al. 1996, Machalski et al. 2006)

As a by-product in previous searches for GRGs a new class of radio sources has been defined which show clear evidence for two phases of activity, one that has ended and one that has recently started (Lara et al. 1999, Schoenmakers et al. 2000b). The outstanding property is that they consist of two double-lobed radio sources, which are well aligned and centred on a common nucleus. Therefore, these sources were called 'Double-double Radio Galaxies' (DDRGs). Common properties of the currently identified DDRGs are that they are relatively large (i.e. larger than 500 kpc, many of them are actually GRGs) and that the radio power of the inner sources is less than that of the outer sources. Recently, Brocksopp et al. (2007) even discovered a 'triple-double' radio galaxy, i.e. a radio galaxy with three pairs of lobes deriving from different epochs of the central AGN activity. Kaiser et al. (2000) presented a scenario for the formation of DDRGs which is based on the occurrence of a short (i.e. lasting for a few Myr at most) interruption of the jet flow in the AGN. Their model basically foresees that a new internal lobe system can develop in the cocoon inflated by the original jets, if this has been enriched by warm and dense clouds from the ambient IGM. There is also growing evidence that the DDRGs are just one possible manifestation of recurrent activity in radio galaxies. Several other morphological types exist (X-shaped sources, VirA-type sources) which might have

their origin in the still visible remainders of a frequent sequence of several duty-cycles of radio activity. It is thus well possible that many more GRGs exist which have not been discovered yet because of the extremely steep spectra of their fading radio lobes.

A pressing problem both in the research of GRGs as probes of the IGM as well as in the study of recurrent activity is the small number of known sources, which seriously hampers testing of the models mentioned above, in particular with statistical methods.

As both types of source are characterised by very extended, diffuse emission with low surface brightness and very steep spectrum, it is presumed that even surveys as low as 325 MHz (WENSS) have missed many of these sources. Large-area surveys at LOFAR frequencies are thus ideal to increase, and probably even complete, the number of known GRGs and recurrent objects for a comprehensive study of these sources instrumental for a proper understanding of radio galaxy evolution.

Furthermore, the higher the number of these faint objects, the higher the probability to find new, rare, objects.

4.5 Dying Radio sources

4.5.1 The last phase in the life of a radio source

Dying radio galaxies represent an interesting, but still largely unexplored, stage of the active galactic nuclei evolution. During their active stage, which may last several 10^7 years, the strong radio sources associated with elliptical galaxies are supplied with energy from active galactic nuclei via plasma beams or jets. Due to the continuous accumulation of new particles, the total spectra of the active radio sources are usually well approximated by a power law over a wide range of frequencies. The injection of energy also sustains the growth of these radio sources which is governed by the balance between the internal pressure in the radio lobes and the pressure in the hot X-ray emitting external medium in which they must expand (Scheuer 1974).

At some point, however, the activity in the nuclei stops or falls to such a low level that the plasma outflow can no longer be sustained and the radio source is expected

to undergo a period of fading (dying phase) before it disappears completely. In the dying phase, radio core, well-defined jets and compact hot-spots will disappear because they are the structures produced by continuing activity. On the other hand, the radio lobes may still remain detectable for a long time if they are subject only to radiative losses of the relativistic electrons.

Indeed, given the comparatively short duration of the radio galaxy phenomenon, we could expect a large number of dying radio sources. However, only a handful of dying radio galaxies in this evolutionary stage are known. According to Giovannini et al. (1988) only few percent of the radio sources in the B2 and 3C samples have the characteristics of a dying radio galaxy.

4.5.2 The spectral evolution of dying sources

A possible explanation for the rarity of the dying radio galaxies may be the relatively fast spectral evolution they undergo during the fading phase. Synchrotron losses and the inverse Compton scattering of the Cosmic Microwave Background photons preferentially deplete the high-energy electrons. The fading lobes are expected to have very steep ($\alpha > 1.3$, $S_\nu \propto \nu^{-\alpha}$) and convex radio spectra characteristic of a population of electrons which have radiated away much of their original energy (Komissarov & Gubanov 1994). In fact, in the absence of fresh particle injection, the high-frequency radio spectrum develops an exponential cutoff. At this point, the adiabatic expansion of the radio lobes will concur to shift this spectral break to lower frequencies and the source will disappear quickly. On the other hand, if the source expansion is somehow reduced, or even stopped, there is still the chance to detect the fossil radio lobe, at least at low frequency.

4.5.3 Dying sources in low-frequency surveys

For the reasons mentioned above, low-frequency selected samples such as the Westerbork Northern Sky Survey (WENSS; Rengelink et al. 1997) at 325 MHz and the B2 survey at 408 MHz (Colla et al. 1975) are particularly well-suited to search for these elusive fossil radio sources. Recently, Parma et al. (2007) by cross-correlating the WENSS with the NVSS (Condon et al. 1998) discovered six new

dying sources and three new restarted sources (see Fig.1). Other two dying galaxies (the central radio source in Abell 2622 and MKW03s) and one possibly restarting source (MKW07) have been recently found by Giacintucci et al. (2007) in a low-frequency survey of nearby cluster of galaxies performed with Giant Metre Radio Telescope. Four more dying sources and one restarting source from the WENSS and the B2 catalogues are presented in Murgia et al. (2008).

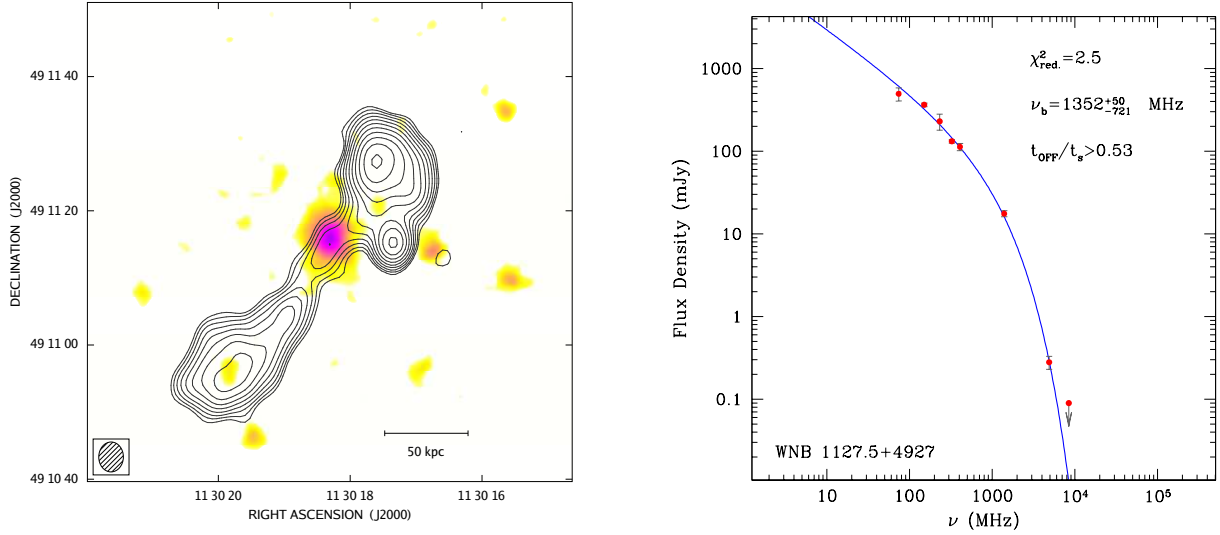


Figure 4.1: Left: Very Large Array image at 1400 MHz of the dying radio galaxy WNB 1127.5+4927 overlaid to the optical image from the Digitalized Sky Survey (from Parma et al. 2007). Right: The exponential cut-off of the integrated radio spectrum at $\nu_{br} \simeq 1300$ MHz indicates that the electron injection is switched off in this source. Compare with the typical active radio galaxies which have power law spectra with $\alpha \simeq 0.8$.

4.5.4 The impact of LOFAR

It is likely that the number of dying galaxies discovered so far is limited by the scarce sensitivity of the current low-frequency surveys, i.e. they could represent just the tip of the iceberg. The radio telescopes of the next generation will reach milli-Jansky sensitivity at frequencies as low as 10 MHz and micro-Jansky sensitivity around 100 MHz. We may expect the discovery of a large population of dying radio sources that have been missed from the current surveys because of their faintness and very steep spectra. These sources are very faint at centimeter wavelengths but should still be

visible at frequency below 100 MHz if they are only subject to radiative losses. Due to its sensitivity, the LOFAR represents the ideal instruments to discover a large number of these elusive objects. At the same time, it will be important to extend the angular resolution of the array down to the arcsecond scale even at the lowest frequencies. In this case it will be possible to study in detail the spectral properties of dying sources along their lobes, shading more light on the last phase in the life of a radio source.

Chapter 5

Galaxy Clusters

5.1 Radio Halos and Relics

The radio emission from galaxy clusters can be broadly divided into two main classes: **(a)** radio sources associated with individual galaxies (or AGNs), or with buoyant relativistic bubbles released by nuclear activity of active galaxies at cluster centers; **(b)** diffuse radio emission, not associated with galaxies, but rather connected to the intracluster gas.

Here we will focus on the diffuse cluster sources **(b)**, whose nature and spectral properties make them a special target for the low frequency range offered by LOFAR.

A fraction of galaxy clusters hosts radio emission of very low surface brightness (of the order of $\mu\text{Jy/b}$), whose extension may reach and exceed the Mpc. Such radio sources, known as ‘radio halos’ (Fig. 5.1) if located at the cluster centre, or ‘relics’ if located in peripheral cluster regions, are characterised by a steep radio spectrum of synchrotron origin ($\alpha \geq 1.2$, for $S \propto \nu^{-\alpha}$; Feretti 2003, Ferrari et al. 2008). Their non-thermal nature proves the existence of micro Gauss magnetic fields and of relativistic particles spread over the whole cluster volume. Radio halos show a fairly regular shape, and their extent and morphology is usually in good agreement with that of the thermal emission coming from the X-ray intracluster gas (e.g. Govoni et al. 2001); relics are polarized and elongated radio sources showing a variety of morphologies, the most common being arcs and toroids. Due to their steep spectrum and low surface brightness, such sources are best imaged at frequencies $\nu \leq 1.4$ GHz and at resolutions \geq few tens of arcsecond.

The origin of diffuse cluster sources has always been a puzzle: their very large extent requires diffusion times largely exceeding the radiative times of the emitting electrons, thus requiring some form of particle acceleration. Radio relics may be associated to shock waves which are unavoidably formed during merger events (*e.g.* Enßlin et al. 1998; Röttiger et al. 1999; Enßlin & Gopal-Krishna 2001) but our understanding of their origin is still limited since only a handful of radio relics have been observed in some details.

On the other hand several progress has been made in our understanding of the origin of radio halos thanks to the increasing number of well studied radio halos and to the analysis of statistical sample. From these studies is becoming clear that radio halos are rare (about 25 known so far) and currently found only in a fraction of massive galaxy clusters with signature of recent (or ongoing) cluster merger (Buote 2001, Venturi et al. 2008). A number of correlations relating thermal to non-thermal cluster observables (*i.e.* radio halo luminosity to cluster X-ray luminosity, or mass or temperature) have been found for clusters with radio halos providing further support to the radio halo/cluster merger connection (Govoni et al. 2004, Cassano et al. 2007). This Mpc-scale radiation may originate from *secondary electrons* injected by collisions between relativistic and thermal protons in galaxy clusters (e.g. Dennison 1980; Blasi & Colafrancesco 1999), alternatively it has been proposed that extended radio emission may originate from relativistic electrons *re-accelerated in situ* by various mechanisms associated with the turbulence in massive merger events (e.g. Brunetti et al. 2001; Petrosian 2001; Fujita et al. 2003). These two processes likely happen at the same time and a unified scenario that model both the injection and re-acceleration of *secondary electrons* and *primary particles* due to MHD turbulence in galaxy clusters has been investigated by Brunetti & Blasi (2005).

Radio Halos are not common: although a fairly large number of clusters has an adequate radio follow up, they are presently detected only in a fraction of massive galaxy clusters with ongoing merger activity (Giovannini et al. 1999; Buote 2001; Cassano et al. 2008; Venturi et al. 2008). This suggests that Radio Halos are *transient* phenomena (the life-time of Radio Halos must be much shorter, < 1 Gyr, than the cluster life-time) connected with cluster mergers and that some threshold

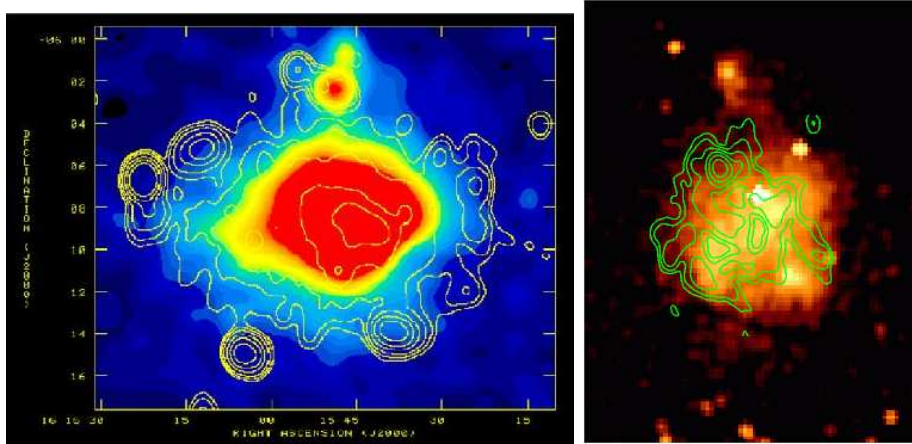


Figure 5.1: Examples of Radio Halos : Abell 2163 (left; Feretti et al. 2001) and RXCJ2003 (right; Venturi et al. 2007; Giacintucci et al. in prep). Contours give the radio emission, colour gives the X-ray emission.

in the mechanism for the generation of these sources should come into play. Unless we admit the *ad hoc* possibility of strong dissipation of the magnetic field in clusters, these properties cannot be easily understood in the case that continuous injection of *secondary* electrons in the IGM plays the major role in the origin of these sources, while they support the idea that turbulent re-acceleration of relativistic electrons may play an important role. This last possibility is also supported by the cut off found at GHz frequencies in the spectrum of the Coma Radio Halo (Schlickeiser et al. 1987; Thierbach et al. 2003).

5.2 Radio Surveys of Galaxy Clusters

Most of the radio halos and relics have been discovered through follow up observations of candidate clusters, extracted from X-ray selected galaxy cluster catalogues, with hint of diffuse radio emission in radio surveys carried out with the main radio arrays, i.e. the NRAO VLA Sky Survey (NVSS) at 1.4 GHz (Giovannini et al. 1999) and the Westerbork Northern Sky Survey (WENSS) at 327 MHz (Kempner & Sarazin 2000). These studies have suggested that diffuse radio emission in galaxy clusters is not common and associated with luminous (massive) clusters

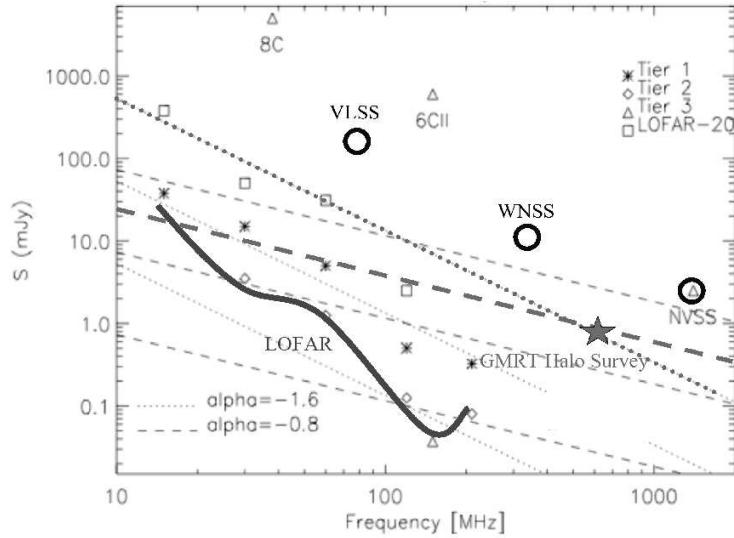


Figure 5.2: Sensitivity of different surveys is reported as a function of frequency. The star symbol gives the sensitivity of the GMRT pointed-survey at 610 MHz to diffuse emission on 45x45 arcsec scale. This is compared to the NVSS brightness sensitivity, and to the WNSS and VLSS surveys sensitivity to diffuse emission on the same 45x45 arcsec scale. Thick solid line gives the LOFAR brightness sensitivity at the different frequencies. Dotted and dashed lines show the evolution in the diagram of the flux of sources with spectrum $\alpha = 1.6$ and 0.8 , respectively.

with complex dynamics.

More recently, a pointed radio survey was designed to firmly establish the statistical behaviour of the diffuse cluster emission by observing, with the GMRT at 610 MHz, about 50 galaxy clusters with luminosity $L_X \geq 5 \times 10^{44}$ erg/s and redshift in the range 0.2-0.4: the GMRT Radio Halo Survey (Venturi et al. 2007 & 2008). The configuration of the GMRT ensures both the detection of diffuse radio emission spread over few arcminutes, and the high resolution necessary to discriminate between genuine diffuse emission and blending of individual sources. The sensitivity level of the GMRT observations is in the range $35 - 100 \mu\text{Jy}/\text{b}$, improving by about an order of magnitude the sensitivity of the NVSS (Figure 5.2). Despite this unprecedented sensitivity no hint of diffuse radio emission is found in the majority of galaxy clusters in the GMRT sample allowing to the discovery of cluster radio-X bimodality : clusters either host a radio halo whose radio power correlates with the

X-ray luminosity (following the radio-X correlation), or the upper limits to their diffuse radio emission are one order of magnitude lower than the level of the radio-X correlation (Brunetti et al., 2007).

Based on the radio-X correlation, radio halos in galaxy clusters with X-ray luminosities lower than a few times 10^{44} erg/s should be faint and not accessible to present radio surveys (e.g. Clarke 2005). Remarkably, it has been claimed that the fraction of cluster with radio halos at 1.4 GHz increases with the cluster X-ray luminosity (Cassano et al. 2008). The LOFAR surveys will reach unprecedented sensitivities at different frequencies (60, 120, 240 MHz; Figure 5.2) allowing to understand whether radio halos form in clusters of lower X-ray luminosity, to constrain the evolution of the occurrence of radio halos in galaxy clusters with cosmic time and to catch the first radio halos that may form at relatively high redshift.

5.3 The Ultra-Steep-Spectrum Radio Halos

In the context of the turbulent re-acceleration scenario, a radio break (or cut-off) is expected in the synchrotron spectrum of radio halos. The frequency of this cut-off depends on the acceleration efficiency (depending in turn on the energy flux of the MHD turbulence dissipated into particle acceleration) and on the strength of the magnetic field in the ICM. The spectral cut-off affects our ability to detect radio halos, introducing a strong bias against observing them at frequencies substantially larger than the cut-off frequency. Presently known radio halos are observed at GHz frequencies requiring an efficient turbulent acceleration mechanism. These halos must result from the rare, most energetic merging events and therefore be hosted only in the most massive and hot clusters (Cassano & Brunetti 2005; Cassano et al. 2006). On the other hand, the majority of radio halos should be formed during much more common but less energetic merging events, for example between a massive cluster and a much smaller sub-cluster (with mass ratio > 5) or between two similar clusters with mass $\leq 10^{15}$ solar masses (Cassano et al. 2006). However these sources, with a cut off in the synchrotron spectrum at $\nu_c < 1$ GHz, would be visible only at lower frequencies because of their ultra steep spectral slope. Thus the discovery of

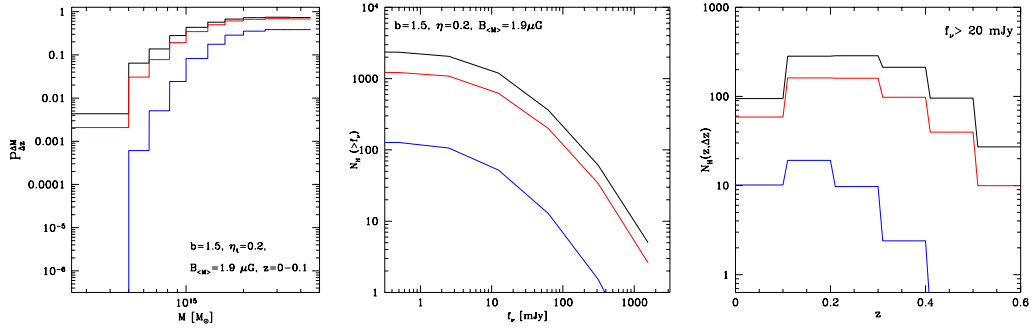


Figure 5.3: **a)** Expected fraction of clusters with radio halos at three radio frequencies: 1.4 GHz (blue lines), 240 MHz (red lines) and 150 MHz (black lines) in the redshift bin $z \sim 0 - 0.1$; **b)** integrated number counts of clusters with radio halos at three radio frequencies: 1.4 GHz (blue lines), 240 MHz (red lines) and 150 MHz (black lines); **c)** number counts of radio halos with flux larger than 20 mJy in different redshift intervals at three radio frequencies: 1.4 GHz (blue lines), 240 MHz (red lines) and 150 MHz (black lines). All calculations have been performed assuming: $b = 1.5$, $B_{<M>} = 1.9 \mu\text{G}$ and $\eta_t = 0.18$.

diffuse Mpc scale emission at a few hundred MHz in galaxy clusters which show no hint of diffuse emission (radio halos) at GHz frequencies, represents a crucial test of the re-acceleration model and a unique step forward in our understanding of the non-thermal emission in galaxy clusters.

Model predictions are illustrated in Fig.5.3a) that reports the expected fraction of cluster with radio halos at different radio frequencies (1.4 GHz, 240 MHz and 150 MHz, see figure caption). A large increase of the fraction of clusters with radio halos at low radio frequencies (240-150 MHz) is expected; this increase is even more striking for the less massive clusters, *i.e.* $M < 10^{15} M_{\odot}$. Fig.5.3b) reports the expected integral number counts of radio halos from a full sky coverage above a given radio flux at 1.4 GHz, 240 MHz and 150 MHz (see figure caption) up to a redshift $z \sim 0.7$. The expected number of radio halos at 150-240 MHz are a factor of ~ 10 larger than the number expected at 1.4 GHz, with the bulk of GRHs at fluxes \geq few mJy. LOFAR will be able to detect diffuse emission on Mpc scale at 150 MHz down to these fluxes and this would be sufficient to catch the bulk of these GRHs. Fig.5.3c) reports the expected number of radio halos with flux larger than 20 mJy

in different redshift interval and at different frequencies (1.4 GHz, 240 MHz and 150 MHz see figure caption). While the bulk of radio halos at 1.4 GHz is expected at relatively low redshift, 0.1 – 0.3, a sizeable number of radio halos is expected to be discovered at higher redshifts at lower frequencies and LOFAR should discover these radio halos.

5.4 Broad band non thermal cluster emission and synergies with observations in other bands

The non thermal emission from galaxy clusters is expected to have a complex behaviour since several components may come up. Particles may be accelerated during cluster mergers via shock and turbulence and this gives a complex population of primary relativistic electrons and protons in the IGM (e.g. Ensslin et al. 1998; Sarazin 1999; Blasi 2001; Brunetti et al. 2001, 2004; Petrosian 2001; Miniati et al. 2001; Ryu et al. 2003; Dolag 2006; Brunetti & Lazarian 2007; Pfrommer 2008). Proton-proton collisions in the IGM give gamma ray emission due to the decay of secondary π^0 and inject secondary electrons that emit synchrotron and inverse Compton (IC) radiation at some level. MHD turbulence may re-accelerate both primary and secondary particles during cluster mergers and this is expected to considerably boost up the synchrotron and IC emission by orders of magnitude in the case of merging clusters (e.g. Brunetti 2004; Petrosian & Bykov 2008).

The non-thermal emission from the central Mpc regions of galaxy clusters is a mixture of two main spectral components: a long-living one that is emitted by secondary particles (and by π^0 decay) continuously generated during p-p collisions in the IGM, and a transient component that may be due to the re-acceleration of relativistic particles by MHD turbulence generated (and then dissipated) in cluster mergers (Brunetti 2008). An example of the expected broad band emission is reported in Fig.5.4 for a Coma-like cluster. Upper panels show the non-thermal emission (synchrotron, IC, π^0 decay) generated during a cluster merger, while lower panels show the emission as expected after 1 Gyr from the time at which turbulence is dissipated. Radio Halos and hard X-ray tails are expected to be produced during mergers, while a long living gamma ray emission is expected to be common in galaxy

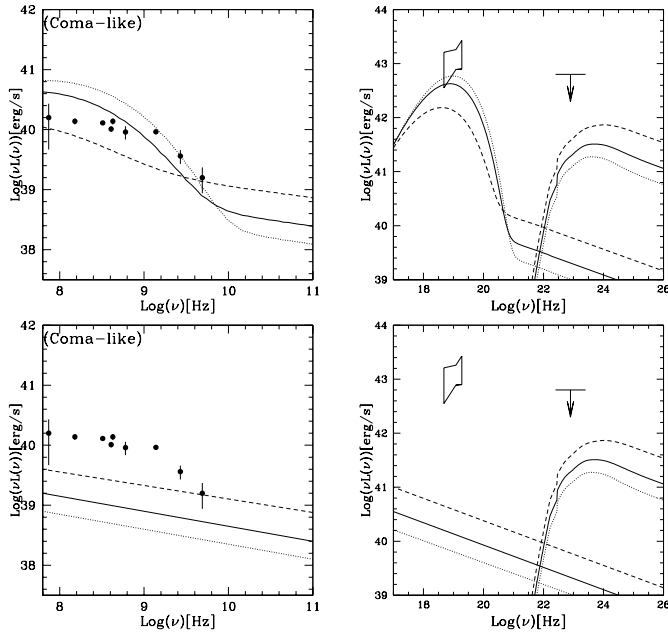


Figure 5.4: Broad band spectrum for a Coma-like cluster accounting for synchrotron (left), and IC and π^o (right) components. Upper panels report the case of a merging turbulent galaxy cluster, lower panel report expectations for non turbulent galaxy clusters (see Brunetti 2008 for details).

clusters.

Only upper limits to the gamma ray emission from galaxy clusters have been obtained so far (Reimer et al. 2003), however the FERMI Gamma-ray telescope (formely GLAST) and the Cerenkov arrays (MAGIC, HESS, VERITAS) will shortly obtain first detections of galaxy clusters or put stringent constraints to the energy density of the relativistic protons. In addition Fig.5.4 shows that a direct correlation is expected between Radio Halos and IC emission in the hard X-rays since the two spectral components are emitted by (essentially) the same population of relativistic electrons: because the ratio between IC and radio luminosity depends on the magnetic field in the IGM, future hard X-ray telescopes (Simbol-X, NuSTAR and Next) will detect a fairly large number of clusters with Radio Halos if the IGM is magnetised at $\approx 1\mu\text{G}$ level (or lower).

The italian communittee is presently involved in the FERMI and MAGIC

collaboration and in the development of the French-Italian-German Simbol-X mission. All these instrument represent a natural complement to LOFAR observations of galaxy clusters.

5.5 Thomson scattering of a cluster central radio source

The central regions of the clusters with cooling cores host large column densities of ionized material, as directly derived by the observations. These regions are likely to be optically thin, with typical values of the optical depth due to electron scattering of $\sim 10^{-2}$. If a powerful radio galaxy resides at the center of a cooling core cluster, we expect that the diffuse radiation originally emitted by the active nucleus will be scattered by the hot electrons in the cooling core region.

The theory of Thomson scattering in cluster cores has been described by Sunyaev (1982) and Wise & Sarazin (1990). Electron scattering is independent of photon frequency. Therefore, the scattered radiation may in principle be detectable in any part of the spectrum. However, it is unlikely that such faint diffuse emission could be detected in the presence of other significant emissions. Radio observations seem to be very suitable to observe this effect, particularly since a very high dynamic range is attainable.

The hydrodynamical state and the ultimate fate of the cooling gas is still uncertain and so a detailed characterization of the profiles of cluster physical properties is still missing. Assuming for simplicity that the cluster gas follows a King model, the intensity of the scattered radiation has the behaviour reported in Fig. 5.5 and the distribution of the brightness temperature is given by the equation (Sunyaev 1982):

$$T_b = 0.92 \left(\frac{S_\nu}{10 \text{ Jy}} \right) \left(\frac{\lambda}{6 \text{ cm}} \right)^2 \left(\frac{10'}{\theta_c} \right) \left(\frac{\tau_T}{10^{-2}} \right) f\left(\frac{\theta}{\theta_c}\right) \text{ mK};$$

here S_ν denotes the monochromatic flux density, θ is the scattering angle (see Sunyaev 1982 for an accurate definition of the geometry of the scattering), θ_c is

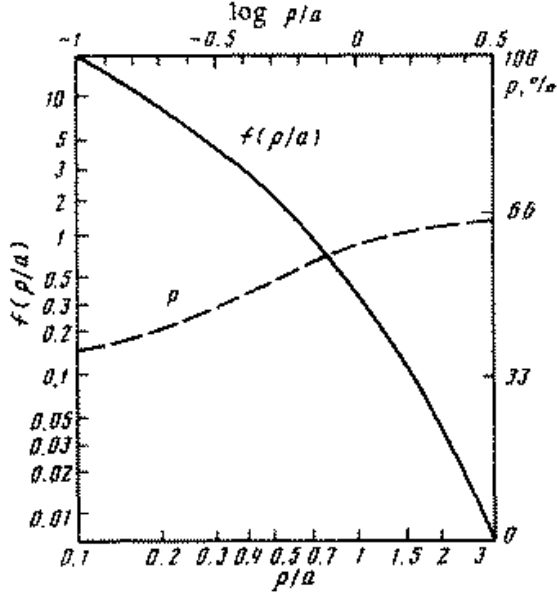


Figure 5.5: Solid curve: dependence of the diffuse scattered radiation intensity on the projected distance ρ from the compact radio source at the center of a cluster of core radius a . Dashed curve: percentage polarization degree of the diffuse radiation as a function of ρ/a (from Sunyaev 1982).

the angular core radius of the cluster, τ_T is the maximum optical depth of the cluster; the function $f(\frac{\theta}{\theta_c}) = f(\frac{\rho}{a})$ is plotted in Fig. 5.5. It is estimated that about 1% of the luminosity of the cluster central source will be scattered (see also Wise & Sarazin 1990).

We can use the above formula to estimate the intensity of the Thomson scattering effect. For example, we obtain that the brightness temperature at 100 MHz (300 cm) from the scattered radiation of a source of 10 Jy has a central peak of ≈ 35 K and falls off very rapidly with distance, as shown in Fig. 5.5. Therefore, the inner regions produce the main contribution to the overall signal: it comes to be at levels of $\approx 10 - 100$ mJy at 100 MHz. Note that both the brightness temperature close to the center and the signal integrated over the source are well above the LOFAR sensitivity and then clearly accessible to LOFAR.

5.5.1 Multifrequency complementarity

X-ray cluster observations from many space observatories (e.g. UHURU, HEAO-1 A2, EINSTEIN, ROSAT, ASCA, Beppo SAX, Chandra, XMM, *Symbol-X*, XEUS, ...) allow to measure the X-ray surface brightness,

$$b_X(E) = \frac{1}{4\pi(1+z)^3} \int n_e^2(r) \Lambda(E, T_e) dl, \quad (5.1)$$

where Λ is the spectral emissivity, being so sensitive to a quantity almost proportional the product of $n_e^2 \times L$ by a well known (frequency dependent) function of the electron temperature; here L is the cluster size.

Microwave observations are sensitive to the SZ effect (Sunyaev & Zeldovich 1972; Zeldovich & Sunyaev 1969; Rephaeli 1995), both thermal and kinematic. *Planck* will provide integrated information on the cluster Comptonization parameter, which quantifies the amplitude of the thermal SZ effect, while higher resolution observations (for example with ALMA) will produce cluster SZ effect detailed mapping of the SZ effect towards the cluster. *Planck* will represent a significant improvement in this field with respect to WMAP, thanks to its better sensitivity per pixel (achieving an improvement of a factor from $\sim 3 - 5$ at $\nu \leq 70$ GHz up to ~ 10 at $\nu \leq 100 - 350$ GHz, according to the exact mission durations), and its better resolution and wider frequency coverage¹ which allows to observe the thermal SZ effect both as a decrement and as an excess over the CMB temperature, other than a better foreground subtraction. Also the $\sim 5'$ (FWHM) resolution channel at 217 GHz, where the thermal SZ drops out and the kinetic one has its maximum, will be crucial to disentangle between these two kinds of effects. Note that the cluster Comptonization parameter is sensitive to the product $n_e \times T_e \times L$. The determination of the number of clusters observable with *Planck* under realistic conditions is under refinement, depending on the global instrument performance and overall data analysis quality, from systematic removal to component separation and source identification. Current estimates predict the identification of about 3000-5000 clusters.

¹*Planck* Collaboration: The Scientific Programme of *Planck*. ESA-SCI(2005)1 [astro-ph/0604069]

In addition, *Planck* will provide a very precise determination of the Hubble constant and of all the other main cosmological parameters (see ESA-SCI(2005)1), allowing to accurately determine the cluster distance from a direct redshift measurement.

As discussed in the previous section, the effect considered here is sensitive to the product of $\sim n_e \times L$ by the source intrinsic brightness.

Collecting the large multifrequency information in these three frequency domains and complementing them with (for example, optical) redshift observations, will allow to achieve an accurate comprehension of both the intrinsic source brightness and spectral energy distribution and the physical and geometrical properties of the IGM surrounding the source.

5.5.2 Polarization

A crucial diagnostic of the scattered radiation is the polarization. Fig. 5.5 reports also the percentage polarization degree of the diffuse radiation as a function of ρ/a , according to the model of (Sunyaev 1982). This emission should be characterized by a high degree of linear polarization, with tangential orientation, and polarization degree increasing with the distance from the cluster center.

Note that both *Planck* (except for its two highest frequency channels at 545 and 857 GHz) and LOFAR will be able to measure also the linear polarization signal.

Chapter 6

Large Scale Magnetic Fields

6.1 Introduction

Observations indicate that most of the Universe is permeated by magnetic fields. Celestial objects are magnetized and magnetic fields of significant strength are found everywhere over small and very large scales, in the interstellar space and in the extragalactic universe. In general, small compact objects have the largest magnetic field strengths, while bigger low-density objects have weaker magnetic fields.

The magnetic fields that we observe in the local Universe probably owe their present strength to dynamo amplification. In many astrophysical contexts, the dynamical scales are very short, thus even a very small primordial magnetic field may be largely amplified through a huge number of e-foldings. The magnetic fields on large-scale, instead, pose a more challenging problem, because the dynamical scales for large-scale objects are long, and thus the amplification is correspondingly slow. This implies the need for seed fields of non negligible intensity; on the contrary, there are good reasons to expect very small fields in the early Universe (e.g., Rees 2006, and references therein). In this framework, it is very important to derive firm values of the large-scale magnetic fields in clusters and in the intergalactic space, in order to constrain the values of seed fields that may have been at their origin and thus constrain the evolution of magnetic fields in the Universe. Clusters of galaxies, being the largest systems in the Universe, represent an ideal laboratory to test theories for the origin of extragalactic magnetic fields.

The investigation of cosmic magnetic fields and of their origin and evolution has

been identified as one of the LOFAR Key Science Projects (PI Rainer Beck).

6.2 Observational diagnostics of magnetic fields

6.2.1 Synchrotron diffuse emission

The presence of magnetic fields is directly demonstrated by the existence of radio emission of synchrotron origin. The total intensity is related to the strength of the magnetic field, while the polarized intensity gives information about: i) the orientation of the magnetic field in the plane of the sky (from the polarization position angle), ii) the field degree of ordering (from the polarization percentage).

From radio data, it is possible to derive an estimate of the magnetic field strength under the assumption of equipartition conditions. The calculations typically assume equal energy in relativistic protons and electrons ($k = 1$), a volume filling factor $\Phi = 1$, a low frequency cut-off of 10 MHz, and a high frequency cut-off of 10 GHz.

6.2.2 Rotation measure

The analysis of the Faraday rotation induced on radio sources from an intervening medium provides an indirect method to derive the strength and structure of the field along the line of sight, as shortly illustrated below.

The synchrotron radiation from cosmic radio sources is well known to be linearly polarized. A linearly polarized wave of wavelength λ , traveling from a radio source through a magnetized medium, experiences a phase shift of the left versus right circularly polarized components of the wavefront. This leads to a rotation $\Delta\chi$ of the position angle of the polarization with respect to the intrinsic (zero wavelength) position angle, according to the law:

$$\Delta\chi = \text{RM}\lambda^2, \quad (6.1)$$

where RM is the Faraday rotation measure. The RM is related to the electron density n_e , in cm^{-3} , and to the magnetic field along the line of sight B_{\parallel} , in μG , through the relation:

$$\text{RM} = 812 \int_0^L n_e B_{\parallel} dl \quad \text{rad m}^{-2}, \quad (6.2)$$

where the path length l is in kpc. By convention, RM is positive (negative) for a magnetic field directed toward (away from) the observer.

The RM values can be derived from multifrequency polarimetric observations of sources within or behind a magnetized medium, by measuring the position angle χ of the polarized radiation as a function of wavelength. In general, the position angle must be measured at three or more wavelengths in order to determine RM accurately and remove the position angle ambiguity: $\chi_{true} = \chi_{obs} \pm n\pi$. The RM value can be combined with measurements of n_e to estimate the cluster magnetic field along the line of sight.

6.3 Magnetic fields in clusters

The study of cluster magnetic fields has gained a big interest in recent years, leading to several new observations as well as simulations. There are, however, still many questions to answer: does the field strength depend on cluster parameters such as the gas temperature, metallicity, mass, substructure and density profile, how do the fields extend, what is the radial trend of the field intensity, what are the coherence scales, how do the fields evolve with cosmic time, and finally how were the fields generated?

The presence of magnetic fields in clusters is directly demonstrated by the existence of large-scale diffuse radio sources which are related to the intracluster medium (ICM) rather than to individual radio galaxies. These sources are known as radio halos and relics (see reviews by Giovannini & Feretti 2004, Feretti 2005 and Feretti & Giovannini 2008). From radio data, it is derived that under equipartition conditions magnetic field strengths in cluster halos and relics range from $\simeq 0.1$ to $1 \mu\text{G}$. Polarized filaments have been detected in the radio halo of A2255 (Govoni et al. 2005). In A 2256, high fractional polarization in the relic indicates large regions (500 kpc) of fairly uniform magnetic field direction (Clarke et al. 2006).

Studies of the Rotation Measure of radio galaxies located within or behind

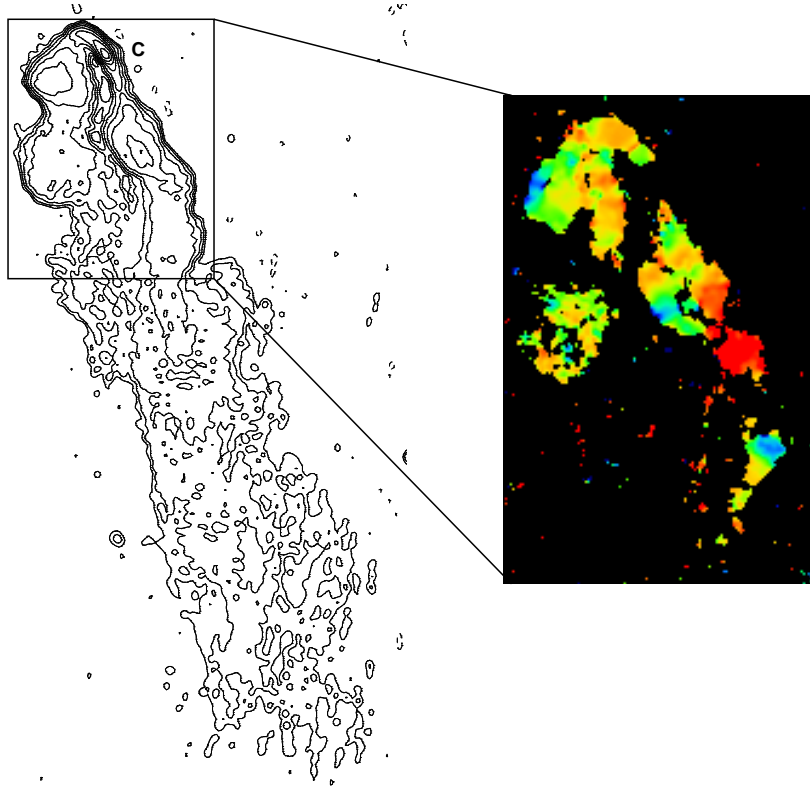


Figure 6.1: VLA contour plot of the tailed radio galaxy 0053-015 in A 119 at 1.4 GHz (left), and RM image (right). The values of RM range between -350 rad m^{-2} and $+450 \text{ rad m}^{-2}$, with $\langle \text{RM} \rangle = +28 \text{ rad m}^{-2}$, and a dispersion of $\sigma_{RM} = 152 \text{ rad m}^{-2}$. They show fluctuations on scales of $\sim 3.5 \text{ arcsec}$ (Feretti et al. 1999).

clusters of galaxies have been carried out on both statistical samples and individual clusters (see e.g. the review by Govoni & Feretti 2004). Values of the Rotation Measure derived with current instruments are of some tens of rad m^{-2} or larger (e.g., Fig. 1).

In simple cases, i.e. if the density and magnetic field strength of the Faraday screen can be approximated by simple geometries, it is possible to derive analytical solutions of the integral (2), in particular when data on radio sources at several cluster locations are available, thus infer the strength of the magnetic field from RM measurements. In more complex and realistic cases, the solution of the integral is not possible analytically and numerical methods or a semianalytical approach are needed (Enßlin & C. Vogt: 2003, Murgia et al. 2004). A recent technique to analyse

and interpret the RM data is the RM Synthesis, developed by Brentjens & De Bruyn (2005), which uses the RM transfer function to solve the $n\pi$ ambiguity related to the RM computation, and allows to distinguish the emission as a function of Faraday depth.

Overall, the data are consistent with cluster atmospheres containing magnetic fields in the range of 1-5 μG , regardless of the presence or not of diffuse radio emission. At the center of cooling core clusters, magnetic field strengths can be larger by more than a factor of 2. The RM distributions are generally patchy, indicating that large-scale magnetic fields are not regularly ordered on cluster scales, but have coherence scales between 1 and 50 kpc. The magnetic field structure can be investigated by deriving the power spectrum of the field fluctuations, defined as: $|B_\kappa|^2 \propto \kappa^{-n}$, where κ represents the wave number of the fluctuation scale. Attempts to derive the value of the power spectrum index have been done by Enßlin & Vogt (2003), Vogt & Enßlin (2003), Murgia et al. (2004), (Govoni et al. 2006).

The magnetic field intensity is likely to decrease with the distance from the cluster center, as derived in Coma (Brunetti et al. 2001). This is also predicted as a result of compression of the magnetic field lines frozen into the thermal plasma during the cluster gravitational collapse (see relation between field strength and gas density in A 119, Dolag et al. 2001).

In most clusters the fields are not dynamically important, with magnetic pressures much lower than the thermal pressures, but the fields may play a fundamental role in the suppression of the particle thermal conduction (Chandran et al. 1999) and in the energy budget of the ICM.

6.4 Magnetic fields in the intergalactic medium

The existence of magnetic fields in the early Universe is demonstrated by the presence of radio sources at very high redshift (up to $z \sim 5$).

Recent attempts to detect diffuse radio emission beyond clusters, i.e. in very rarefied regions of the intergalactic space, have shown recent promise in imaging diffuse synchrotron radiation of very low level. A very faint emission has been detected at 327 MHz in the Coma cluster region (e.g. Kim et al. 1989, Kronberg

2006). The equipartition magnetic field in this region is $\simeq 10^{-7}\text{G}$. Another possible evidence of radio emission in the intergalactic medium is represented by the filament of galaxies ZwCl 2341.1+0000 at $z \sim 0.3$ (Bagchi et al. 2002), several Mpc in size. In addition, the giant ring-like features detected in A 3376 (Bagchi et al. 2006) have been suggested to be related to the large-scale structure formation process, rather than to the cluster.

All these data support the existence of an intergalactic magnetic field more widespread and somewhat lower than that in the intracluster medium within clusters. It could be possibly associated with large-scale shocks related to the formation of the large-scale structure (Keshet et al. 2004). This field may represent the seed field for galaxies and clusters, and may play an important role in the formation of large-scale structure.

Limits to the cosmological magnetic fields of 10^{-8} - 10^{-9} G have been obtained in the literature using different approaches: i) from the the effect of the inhomogeneities in the matter distribution of the Universe on the Faraday rotation of radiation from distant QSOs, for fields coherent across the present horizon (Blasi et al. 1999); ii) from the isotropy of the cosmic background radiation (Barrow et al. 1997).

6.5 Origin of intracluster magnetic fields

The field strengths that we observe in clusters greatly exceed the amplitude of the seed fields produced in the early universe, or fields injected by some mechanism by high redshift objects (Rees 2006). There are two basic possibilities for their origin: i) ejection from galactic winds of normal galaxies or from active and starburst galaxies (Kronberg et al. 1999, Völk & Atoyan: 1999), ii) amplification of seed fields during the cluster formation process.

Support for a galactic injection in the ICM comes from the evidence that a large fraction of the ICM is of galactic origin, since it contains a significant concentration of metals. However, fields in clusters have strengths and coherence size comparable to, and in some cases larger than, galactic fields. Therefore, it seems quite difficult that the magnetic fields in the ICM derive purely from ejection of the galactic fields, without invoking other amplification mechanisms.

Magnetic field amplification is likely to occur during the cluster collapse, simply by compression of an intergalactic field. Clusters have present day overdensities $\rho \sim 10^3$: in order to get $B_{\text{ICM}} > 10^{-6}$ G by adiabatic compression ($B \propto \rho^{2/3}$) requires intergalactic (seed) fields of at least 10^{-8} G. A larger field amplification can be obtained through cluster mergers. From MHD calculations, Dolag et al. (1999) derived that fields can be amplified from seed fields of $\sim 10^{-9}$ G at $z = 15$ to $\sim 10^{-6}$ G at the present epoch. Subramanian et al. (2006) argue that the dynamo action of turbulent motions in the intracluster gas can amplify a random magnetic field by a net factor of 10^4 in 5 Gyr. The field is amplified by random shear, and has an intermittent spatial distribution, making possibly filaments.

Accurate detection of seed fields in the intergalactic medium is crucial to constrain models of magnetic field evolution and amplification.

6.6 Magnetic field studies with LOFAR and eLOFAR

Owing to the low frequency range, LOFAR is particularly suitable to detect diffuse synchrotron emission characterized by steep spectrum. The detection of synchrotron radiation at the lowest possible levels will allow the measurement of magnetic fields in clusters and in even more rarefied regions of the intergalactic space, and the investigation of the relation between the formation of magnetic fields and the formation of the large-scale structure in the universe.

Among RM studies, it follows from Eq. 1 that LOFAR can detect Faraday rotation down to 0.1- 1 rad m^{-2} , owing to the long wavelengths involved. For instance, a RM of 0.1 rad m^{-2} produces between 120 MHz and 240 MHz a rotation of the polarization angle of 27deg, which is easily detected. For comparison, it should be stressed that a RM ≤ 1 rad m^{-2} induces between 1.4 GHz and 5 GHz a rotation of the polarization angle ≤ 2 deg, which is very difficult to measure with the current instruments. The detection of very low rotation measures implies in turn the detection of very faint magnetic fields (Eq. 2), therefore LOFAR will become the radio telescope to measure the weakest cosmic magnetic fields so far.

The high density peaks of the cosmic filaments produced by the gravitational

infall can be detected by mapping the diffuse synchrotron emission arising from a combination of particle acceleration and the extended cosmic magnetic field. LOFAR observations can therefore be used to trace the extended baryon component of the cosmic web. Fields of $B \simeq 10^{-9}$ – 10^{-8} G are expected along filaments of 10 Mpc length with $n_e \simeq 10^{-5}$ cm $^{-3}$ electron density (Kronberg 2006) which yield Faraday rotation measures of $\text{RM} = 0.1$ – 1 rad m $^{-2}$.

To measure such low RMs needs high angular resolution and accurate subtraction of the Galactic foreground and of contaminating discrete radio sources. To this aim, the high angular resolution of eLOFAR is important. RM gradients in the Galactic foreground must be resolved to avoid beam depolarization. High angular resolution is also needed to resolve possible small scale fluctuations in the magnetic field structure: fluctuations of a few kpc, currently detected in nearby clusters, will require arcsec/subarcsec resolution to be detected at $z \sim 0.1 - 0.2$.

6.7 Summary of the LOFAR and eLOFAR specifications

The investigation of large-scale magnetic fields with LOFAR will benefit from the following instrument specifications:

- low frequency range, to allow detection of very low level synchrotron emission of steep spectrum (cluster and intergalactic fields, cosmic web), and to detect low Rotation Measures (and hence faint magnetic fields),
- large field of view, to obtain observations of large portions of the sky in reasonably short times;
- large bandwidth with a large number of channels, to obtain RM values from single frequency observations (surveys);

The high angular resolution supplied by eLOFAR will be crucial to:

- resolve magnetic fields gradients in the Galactic foreground, thus reducing beam depolarization,
- resolve foreground screens due to local turbulence, discrete radio sources, clouds, etc.,

- distinguish between Farady rotation originating along the line of sight in the intervening medium, and that possibly internal within a radio source.

Chapter 7

Studies of the Galactic Magnetism

The magnetic field is an important component of the Interstellar Medium (ISM) and, as in almost any astrophysical context from stars to cosmology, the physics of the Galaxy cannot be studied without accounting for it.

Evidences of a Galactic magnetic field have been found since 1960's (e.g. Westerhout et al. 1962) but its structure, origin and evolution are still unclear. It is now generally accepted that magnetic fields have not a purely primordial origin, but some magneto-hydrodynamics mechanism should have amplified it from some seed field. However, the nature of seeds and the type of dynamo amplification process are still unclear. Understanding the large scale structure of the magnetic field is crucial for disentangling models, since it largely depends on the models details. For instance, a mean-field dynamo would generate a large scale field well extended in the halo (e.g. Brandenburg et al. 1992), while a small scale dynamo would generate a mainly turbulent field with power essentially on small scales (e.g. Subramanian 1998): either the detection or non-detection of a large scale magnetic field in the halo would thus allow us to distinguish between these two models.

7.1 Magnetic fields probes at radio wavelengths

Most of what we know about astrophysical magnetic fields comes from radiowavelengths, where processes related to the magnetism either dominate the emission (synchrotron), or generate measurable effects (Faraday rotation). Four main probes are:

1. The total intensity synchrotron emission, which is related to the total magnetic field (turbulent + ordered component).
2. Its polarized component, which traces the regular field. The polarization fraction measures the ratio between ordered and total magnetic field. The polarization angle, instead, gives the direction of the magnetic field parallel to the plane of sky.
3. The polarization angle ϕ is rotated by Faraday Rotation (FR) with the wavelength square

$$\Delta\phi = \text{RM} \lambda^2 \quad (7.1)$$

where the Rotation Measure RM is

$$\text{RM} = 0.81 \int n_e B_{\parallel} dl \quad (7.2)$$

and measures the magnetic field parallel to the line of sight B_{\parallel} [μG] weighted for the electron density n_e [cm^{-3}] integrated along the path dl [pc]. If n_e can be measured independently (e.g., by X-ray or $\text{H}\alpha$ data), RM gives an direct measurement of B with no theoretical assumption (like equipartition). Multifrequency observations are required. Both diffuse emission and extragalactic point sources can be used, the latter probing a value integrated along the whole line-of-sight (e.g. Brown et al. 2007). RM of pulsars can be used as well with the additional information of their distance from the Sun (e.g. Han et al. 2006).

4. The RM-synthesis is a new technique based on an extension of the RM concept (Brentjens & de Bruyn 2005). It enables a sort of tomography of the magneto-ionic medium and gives how the polarized emission is structured along the line-of-sight. Spectropolarimetric observations are required on a wide band and with high frequency resolution. Key parameters are the RM resolution

$$\delta\phi \sim \frac{2\sqrt{3}}{\Delta\lambda^2} \quad (7.3)$$

and the RM range accessible

$$|\text{RM}|_{\text{max}} \sim \frac{\pi}{\delta\lambda^2} \quad (7.4)$$

where $\Delta\lambda^2$ is the bandwidth and $\delta\lambda^2$ the spectral resolution in λ^2 -space.

7.2 The Galactic Magnetic Field

The study of the magnetic field in the disc of our Galaxy has made significant advances in the last few years. Observations of external spiral galaxies show that the spiral arms are usually dominated by a turbulent or tangled component with a weaker coherent field aligned with the arms. In the inter-arm regions the regular component is more relevant and depicts *magnetic arms* with coherent scales up to the size of the disc (e.g. Beck 2007).

Although the case of our Galaxy is harder to be understood because of our internal location, recent high sensitivity and high spatial density RM data in the Galactic plane has enabled first studies of the 3D structure in the disc (e.g. Haverkorn et al. 2006, Brown et al. 2007). What seems most favoured is a spiral structure down to the molecular ring, where the field gets a ring shape (e.g. Brown et al. 2007, Sun et al. 2008). The field in the local arm is clock-wise as seen from the north Galactic pole, while at least one reversal (inversion of the field heading while keeping the same alignment) seems to take place toward the inner Galaxy. More data are necessary to work out points still under debate (e.g. the number and location of the reversals, and the extension of the ring), but a general consensus on this framework seems to have taken place.

Far less clearer is the case of the halo, instead. This is not only because of the weaker signal, which makes hard to detect the synchrotron emission in this low emitting region, but also of the many different patterns found so far in external galaxies: from galaxies without evident halo field, to X-shaped fields centred at the galaxy centre (e.g. NGC 891, Fig. 7.1 left panel), and up to large almost spherical magnetic halos (e.g. NGC 4631, Fig. 7.1 right panel).

About the halo of our Galaxy, data are far fewer than those in the disc and models are essentially unconstrained. Our knowledge is basically based on RMs of extragalactic sources and pulsars at mid and high Galactic latitudes, which, however, are coarsely and irregularly sampled. Han (2002) finds that RMs values are asymmetric both with respect to the plane and the Galactic centre, which is

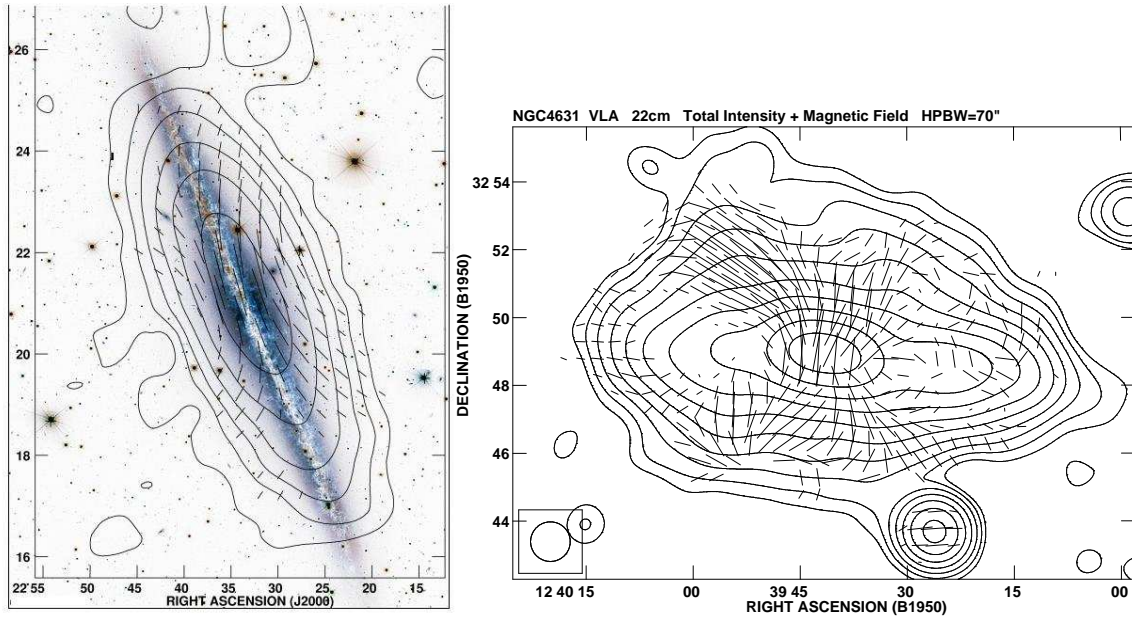


Figure 7.1: **Left:** Radio emission of the galaxy NGC 891 at 8.35 GHz. Total intensity is given by contours, polarized emission by vectors (magnetic angle). Optical image is overlapped. From Krause et al. 2008 (Copyright: MPIfR Bonn). **Right:** Total radio emission at 22 cm of the spiral galaxy NGC 4631 (From Beck 2005). Polarized emission is given by the vectors. (Copyright: MPIfR Bonn).

compatible with a field generated by an α - Ω dynamo model of A0-mode: two toroidal fields above and under the Galactic plane antisymmetric across the plane (sign reversal). However, diffuse polarization maps at 1.4 and 22.8 GHz clearly show very large structures in that region extending from the plane up to high latitudes. These likely are of very local origin, and contamination of RM data by local *anomalies* is possible. Recently, Sun et al. (2008) have used most of the available data but find that their model cannot yet constrain the halo field essentially for lack of data.

As a conclusion, very little is known about the field in the Galactic halo, and far more data are necessary to understand how it is structured.

7.3 Galactic magnetism at low frequencies: LOFAR

Low frequencies are excellently suited for measuring weak magnetic fields and LOFAR can enable crucial advances in measuring and understanding the magnetic field in the Galactic halo.

The synchrotron frequency spectrum of the ISM diffuse emission has a negative power law with a brightness temperature proportional to¹ $\nu^{-(2+\alpha)} B^{(\alpha+3)}$ with $\alpha \sim 0.7$, ν the observing frequency, and B the magnetic field intensity. In case of same sensitivity, that means that at 150 MHz magnetic fields $5\times$ weaker than at 1.4 GHz can be measured. At low frequency the spectrum could flatten for synchrotron self-absorption counterbalancing this benefit, but regions with weak fields are expected to be still optically thin at the LOFAR frequencies making negligible this effect. In principle, the low frequency band of LOFAR allows even better performances ($15\times$ weaker fields at 30 MHz), but the worst sensitivity of the Low Band Antennas (LBA) makes the high band (120-240 MHz) the best choice to detect weak fields with LOFAR.

Lower frequencies not only means weaker fields but also older electrons. The electron lifetime is proportional to $\nu^{-0.5}$, so that electrons emitting at 150 MHz are $3\times$ older than those at 1.4 GHz ($5\times$ at 50 MHz). The vertical scale length of the synchrotron emission is 1-2 kpc at 1.4 GHz, so that only the part of the halo closer to the midplane is emitting. This is likely because of both the weaker fields of the outer halo and the too short lifetime of the relativistic electrons which does not allow them to diffuse out to the entire halo and illuminate the magnetic field. The longer lifetime of the low frequency electrons, instead, might allow them to diffuse into the whole halo. This, along with the better sensitivity to weak fields, might enable LOFAR to probe the magnetic field structure in the entire halo.

Similarly, LOFAR can detect the halo synchrotron emission also in external galaxies. Beside the importance in itself (i.e., to understand the magnetic field of those individual galaxies), this would enable statistical analyses to find out which is the most common and efficient among the processes which generates and sustains galactic magnetic fields. All of this helps also understand the Galactic magnetism,

¹in case of equipartition

1.4 GHz Polarized Intensity

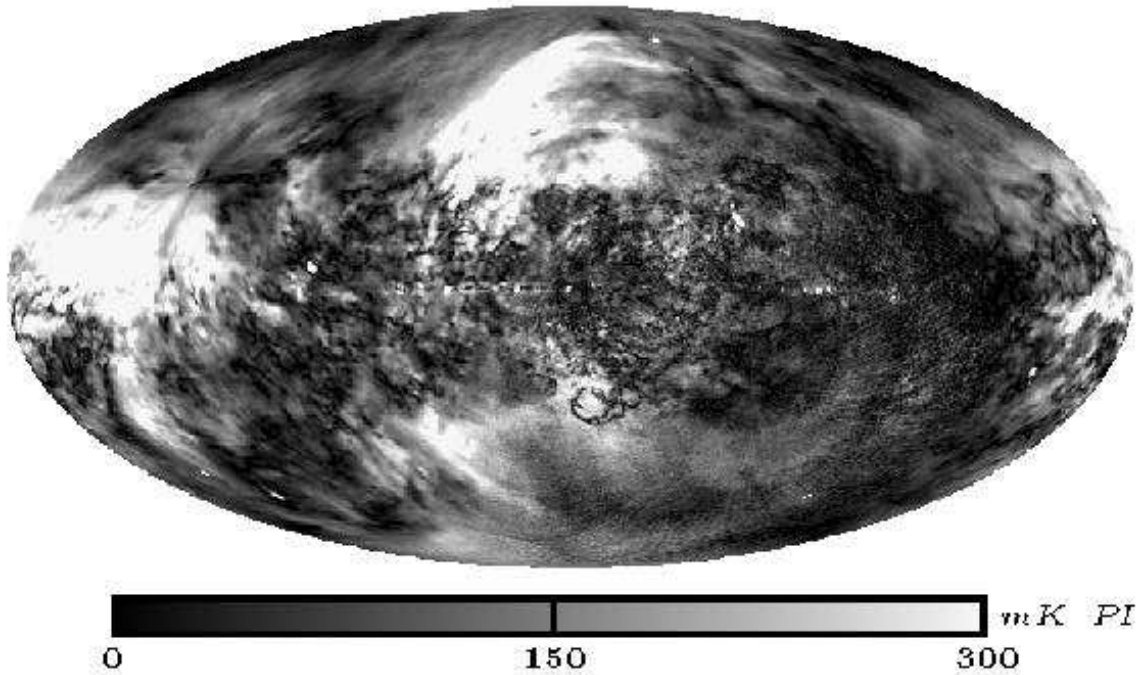


Figure 7.2: All-sky polarized intensity emission map at 1.4 GHz (from Reich 2006). The map is combination of a northern (Wolleben et al. 2006) and southern surveys (Testori et al. 2008).

the external galaxies providing examples which can help interpret the Galaxy case.

The 1.4 GHz all-sky polarization survey (Wolleben et al. 2006, Testori et al. 2008) shows strong depolarization around the Galactic plane at latitude $|b| < 30^\circ$ (Fig. 7.2). A smooth emission features the high latitudes, instead, which are thus marginally affected by Faraday and beam depolarization (36' of angular resolution). Smooth emission in the halo is visible also at lower frequency (408 MHz) even at coarse angular resolution (Carretti et al. 2005 using data by Brouw & Spoelstra 1976). Measurements with higher angular resolution show polarized emission at even lower frequency (350 MHz) already at mid latitudes. This supports that LOFAR, thanks to its excellent angular and spectral resolution, can detect the ISM polarized emission at high latitudes.

But the most powerful tool of LOFAR to investigate weak magnetic fields is the

RM-synthesis, enabled by the low frequency and the excellent spectral resolution of this telescope (1 kHz). In fact, the high frequency band (120-240 MHz) allows an RM resolution of 0.7 rad/m^2 , corresponding to fields as weak as $0.1 \mu\text{G}$, if the entire halo depth can be probed. This RM resolution is well suited for the Galactic halo where RMs range within $[5, 20] \text{ rad/m}^2$. This enables LOFAR to perform a precise and unique tomography of the magneto-ionic ISM with fine details both in angular and Faraday spaces, and, in turn, an accurate study of the 3D structure both of the medium and magnetic field.

LOFAR can thus be a powerful machine to investigate the Galactic halo magnetic field and reveal its structure. LOFAR can give us the first chance to detect the polarized diffuse emission from the whole Galactic halo and probe the magnetic field out to its outer edge, possibly investigating also the transition into the IGM. Even more exciting it is its capability to realise tomographies of the magneto-ionic medium, which enables us to explore the 3D structure of the halo. All of that can reveal us how the large scale structure of the Galactic field is arranged, and, possibly, help constrain the models of the processes which generated and sustains it.

Chapter 8

Radio Pulsar Studies

8.1 Scientific Case

Pulsars are rapidly rotating highly magnetized neutron stars, emitting anisotropic and large band beam(s) of radio-waves, which appear like a pulse, once per star's rotation. Forty-one years of pulsar research have definitely promoted important improvements in a large variety of scientific fields, ranging from physics of ultra-dense matter to electrodynamics, from gravity theories to stellar evolution, from plasma physics to globular cluster dynamics (see Lorimer & Kramer 2004 for a recent review on the possibility of using pulsars as physics tools). Striking examples have been the confirmation (using the original binary pulsar, Hulse & Taylor 1975) of the existence of gravitational radiation, as predicted by Einstein's general theory of relativity and, more recently, using the first Double Pulsar (Burgay et al. 2003, Lyne et al 2004), the possibility of testing various predictions of general relativity in a strong gravitational field at 0.05% level (Kramer et al. 2006).

8.2 The impact of Lofar on pulsar research

There are at least 3 main reasons for investigating pulsars with an instrument like Lofar:

- 1) Pulsars are radio sources with a very steep spectra and are bright just in the radio band where Lofar has an exceptionally high sensitivity. In fact, the average pulsar spectrum is $S \propto \nu^{-\alpha}$ with $\alpha = 1.7$ (where S is the flux

density and ν the frequency of observation) for frequencies greater than about 300 MHz, and peaks in the range 100-300 MHz (Maron et al. 2000). As a consequence the radio pulsars are typically ten (or more) times brighter in the ~ 150 MHz band than at the central frequencies of the major surveys performed so far: ~ 400 MHz or ~ 800 MHz or ~ 1400 MHz. That in turn means that a significant population of pulsar having ultra steep spectrum $\alpha > 3.5 - 4.0$ could have been missed by previous surveys, given the low intrinsic luminosity of such sources at the aforementioned typical survey frequencies. It is particularly interesting that a significant sample of sources is known to have $\alpha > 2.7$, thus displaying a steeper spectrum than the usually adopted scaling of the sky background temperature with respect to the observing frequency $T_{sky} \propto \nu^{-2.7}$. Given that, if a ultra steep spectrum pulsar population exists, it could be easily discovered by a sensitive survey carried on at very low frequencies.

The expectation above is strengthened even more by recent low frequency studies of millisecond pulsars, showing that some of them do not display any peak in the spectrum down to $\nu \simeq 100$ MHz (e.g. Kuzmin & Losovsky 2001). Indeed, inspecting the whole pulsar catalogue, it results that the sensitivity of Lofar is large enough for detecting *single pulses* from between $\sim 25\%$ and $\sim 35\%$ of the total sample of pulsars located in the portion of sky above the horizon of Lofar. This would be an exceptional improvement in the studies of the pulsar radio emission mechanism, whose modelling has been made difficult by the limited number of sources for which single pulses can be observed. In particular single pulses will be detected with high signal-to-noise in about 20 already known millisecond pulsars (plus possibly in many other newly discovered pulsars of this class), an order of magnitude more than the presently available sample. This is particularly interesting because the magnetic field strength and the size of the magnetosphere in the millisecond pulsars are much smaller than for the ordinary pulsars. Therefore the comparison between the physical mechanisms for radio emission in the two classes of pulsars is of primary importance for understanding the working of the radio emission. Similarly, low frequencies are very appealing for investigating

other manifestations of the pulsar emission mechanisms, like the shape of the pulse and its polarization: in fact the frequency evolution of these features appears particularly large just at these frequencies.

2) The wide field of view of Lofar makes it an unprecedentedly good instrument for searches of pulsars and transients. In order to perform searches, the best option is to use the Lofar Core summing the signal from the various stations in an incoherent way. This will guarantee a very good sensitivity (of order 1 mJy at 120 MHz), while preserving a large field of view (about 2 degrees @ 120 MHz). In fact, even accounting for the possibility of multi-beaming, a coherent sum of the signal would make each beam of Lofar far too small (only about 5' @ 120 MHz) for an affordable all-sky search. Simulations show that a survey of the entire Northern Sky may result in the detection of about 1000 pulsars, the majority of them being new discoveries (van Leeuwen & Stappers 2008). This would imply the possibility of doubling the catalogued sample of objects at the Northern celestial declinations. The availability of such an enlarged number of sources will in turn trigger the opening of a new era in the study of the interstellar medium (via the investigation of scattering and dispersion of the radio signal) and of the Galactic magnetic field (via the determination of the Faraday Rotation Measure).

Since the effect of the scattering at the Lofar frequencies is nominally expected to be far worse than at the radio frequencies typically used for pulsar surveys, one may expect that only ordinary pulsars (i.e. sources having spin period longer than few tens of millisecond) will be discovered by Lofar. This is likely not true: on one hand, the huge (with respect to previous surveys) sensitivity of Lofar will give the possibility to sample the faintest end of the luminosity function of those millisecond pulsars (i.e. sources with typical period less than ~ 20 ms) which are relatively close to the Sun (dispersion measure less than about 50 pc/cm^3) and therefore not strongly affected by the scattering of the signal. On another hand, the scattering effect is intrinsically hard to be predicted for a given direction in the sky and there are examples of millisecond pulsars easily detected at low frequencies, despite their dispersion measure

should make their observation in principle impossible.

In fact a most interesting target for Lofar will be the millisecond pulsars harbored in not too far Globular Clusters. In this case a coherent summing of the signal from all the stations in the Core will be adopted, since the size in the sky of the central regions of a Globular Cluster is typically of the order of the synthesized beam of the Lofar Core. With coherent summing, the limiting sensitivity will reach ~ 0.2 mJy @ 120 MHz.

Furthermore, Lofar will be the first instrument having enough sensitivity to perform a search for pulsars (at least for those in the upper end of the pulsar luminosity function) in external galaxies, like M33 and Andromeda. In particular, the most star rich part of the latter galaxy can be entirely covered by only 7 beams of the Lofar Core, enabling the adoption of a very long integration time for each of the pointings.

Last, but certainly not the least, the wide beam of Lofar, coupled with the possibility of performing multi-beaming, will make this instrument a wonderful tool for studying transient radio emitters, like the recently discovered Rotating Radio Transients (RRATs) or extragalactic bursting sources.

3) The multi-beaming capabilities of Lofar, as well as the possibility of tuning sub-array on different frequencies, allow the researchers to perform new kinds of observations over a large sample of radio pulsars. In particular, using various sub-groups of stations, one can simultaneously observe a source over a wide range of frequencies, from 30 up to 240 MHz, allowing for the first time him/her to investigate short time scale variations in the pulsar spectral index, as well as the connection between these changes and other still unexplained behaviors of the pulsar emission, like Mode Changing (Weltevrede, Stappers & Edwards 2007), and Nulling (Rankin & Stappers 2008). The capability of performing multi-frequency and/or multi-pulsar observation will also open the possibility of investigating on a regular base the so-called *interstellar weather*. This will be a fundamental activity for complementing the high precision pulsar timing experiments (like those searching for the signature of the gravitational wave

background) which will require regular information on the interstellar weather for reaching their maximum accuracy.

8.3 The case for a single station

The investigations reported in the previous section will be possible using the Core of Lofar and/or a relatively large number of stations. Entering the project will of course allow the italian pulsar scientists to have a part (relatively small, but not insignificant) in the data analysis and the scientific exploitation of the aforementioned Lofar activity in the field of pulsar research.

In addition, the availability of a single station may allow the italian researchers to carry on a series of independent (from the rest of the Lofar project) pulsar studies which will be worthwhile by themselves. In particular: **a]** monitoring of objects like intermittent pulsars, to see when they turn on. The nature of these sources is still largely debated and an intense campaign of observation is needed for shedding light on their link with other type of pulsars. **b]** timing observations of glitching pulsars, whose observations are usually largely spaced in time at the major radio telescopes, thus preventing to catch up the phases immediately preceding and following the glitch event. An intense campaign of observation may be possible at a single Lofar station, exploiting the large field of view and the very short integration times implied by the use of a low frequency. **c]** high frequency resolution studies of the interstellar medium. Since even a single Lofar station is capable to detect about 130 pulsars with a signal-to-noise of order 25, it can be used for a detailed investigation of the interstellar medium (see previous section) over a large number of line-of-sights.

It is however important to notice again that all the scientific activities reported in this section will require an intense use of the (putative) single station in a standalone mode. Having two or more "national" stations will obviously increase efficiency and scientific pay-back from all the studies.

Chapter 9

Solar-Terrestrial Physics with LOFAR

9.1 Introduction

Solar-Terrestrial Physics (STP) describes the state and evolution of the coupled physical systems that characterize respectively the Sun, the Interplanetary Medium (IPM) and the Earth, and the perturbations that affect them. Different plasma domains and phenomena are relevant to the Sun's inner core, the solar dynamo, the Sub-Photosphere, the Photosphere, the Chromosphere, flares, the Corona, the extended Corona, the Solar Wind, Coronal Mass Ejections (CME), Solar Cosmic Rays (SCR), the Earth's Magnetosphere, the Radiation Belts, the Atmosphere, the Ionosphere. Specifically, the Sun is the primary source of perturbative phenomena, which can propagate through the IPM and reach the Earth. The physical state of such coupled systems is described in terms of Space Weather, which, more specifically, is defined as Solar, Interplanetary, Magnetospheric and Ionospheric Weather, respectively. An extensive review on Space Weather, its drivers and the related models has been carried out in the framework of the European COST Action 724 gDeveloping the Scientific Basis for Monitoring, Modeling and Predicting Space Weatherh (Lilensten et al., 2008). A comprehensive approach includes also the Heliosphere, which is permeated by Galactic Cosmic Rays, whose flux is modulated by the Solar Wind state and therefore by the solar activity level, and which comprehends the other bodies of the Solar System, such as the planets, which interact with solar perturbations at different levels depending on the existence and

characteristics of planetary magnetospheres. Solar activity is driven by the interplay between the solar dynamo and fluid motions of the solar plasma, which rearranges the global and local magnetic field topology, leading to the storage of magnetic energy and its sudden explosive release during reconnection originating particle acceleration and broadband radiation outburst emission in flares or to the release of plasmoids accelerated to the IPM (CME), both phenomena with high probability of being geoeffective, i.e., of transferring energy and perturbing the Geospace. No consistent global model of solar activity exists to date and only a series of event-related models exists for flares and CMEs (Messerotti et al., 2008).

LOFAR can play a fundamental role in diagnosing a variety of phenomena relevant to STP in an almost unexplored electromagnetic domain and with unprecedented spatial resolution as summarized in the following sections.

9.2 Low-Frequency Radio Diagnostics of Solar Phenomena

9.2.1 Solar Radio Bursts

Solar Radio Bursts (SRB) are generated by a variety of thermal and non-thermal, gyrokinetic and plasma processes, which are non- or associated with flares and in the latter case are characterized by specific timings and spatial locations with respect to the associated flare (Best, 2008). Hence, SRBs are effective proxies of:

- Magnetic topology changes (Type I bursts);
- Propagating shocks and particle beams (Type II bursts);
- Particle acceleration and particle beams (Type III bursts);
- Magnetic reconnection and acceleration (Type IV bursts);
- Energy release fragmentation and acceleration (Type IV bursts);
- Radio signatures preceding flares (radio precursors) (Dulk, 1985; Bastian et al., 1998; Messerotti et al., 2003a).

Typically, radio signatures excited in the high corona to the IPM are observed at low frequencies, as the radio emission frequency is related to the local plasma frequency and hence to the local plasma electron density. Low-frequency (LF) diagnostics can be inferred from radio spectra, which provide 2.5D information in the frequency-time domain (e.g., Messerotti, 1998). For instance, the Green Bank Solar Radio Burst Spectrometer (GBSRBS) operates in the range 10-70 MHz and can be used for 2.5D diagnostics in a series of use cases (White et al., 2005;

White, 2007). In particular, the LF signature of: - Storm continuum is indicative of magnetic topology changes in the high corona; - A non-flare-associated Type III burst is determined by a fast propagating electron beam exciting beam-plasma instability, and it contains information about particle acceleration, beam formation, propagation, instability and disruption, plasma state and magnetic field at the source; - A Type III bursts group allows inferences about the associated flare impulsive phase and flare physics; - A Type III followed by a Type V burst show information on triggering agent, emission process, exciter propagation, plasma wave spectra, magnetic topology and flare physics; - A Type III group followed by a Type II burst, generated by a propagating low speed shock, are indicators of shock formation and propagation, beam formation, fine- and large-scale structure of the source and background plasma, association with CMEs and flares; - A Type II burst followed by a Type IV burst are related to the magnetic topology and its evolution, to the associated flare physics, and to the eventual ionospheric response to the associated Extreme UltraViolet (EUV) outburst when a Short-Wave Fadeout (SWF) is observed. A combined imaging analysis of emission associated with a CME in the radio and optical bands (e.g. Bastian et al., 2001) allows the study of the CME onset, formation and propagation, of the shock and beam physics, of the magnetic field and of the flare association.

In this framework, the added value of LOFAR observations is related to its key features that can be summarized as follows in the context of the specific diagnostics: a. The low receiving frequency range corresponds to a $10^8 - 10^7 \text{ cm}^{-3}$ electron density range in the solar corona, i.e., to a radio diagnostics range from 1.15 to 2.5 solar radii; b. The high sensitivity allows the extension of the diagnostic to faint radio signatures; c. The arcsec spatial resolution allows to resolve the radio source spatial structure; d. The sub-second time resolution allows to better sample the radio source evolution; e. The radio imaging capability can map the radio source structure; f. The radio imaging spectroscopy provides the radio source 3D time evolution.

9.2.2 Solar and Interplanetary Plasma Turbulence

Radar diagnostics can get information on both plasma turbulence related to wave emission and propagation as well as to the CME plasmoid. The first solar radar observations in microwaves is documented in Benz and Fitze (1990).

LOFAR can detect low-frequency echoes of radar pulses directed to the solar corona from a suitable transmitting system and the turbulence spectrum of plasma waves in the solar corona can be determined (White et al., 2003; Best, 2007). This is a key factor in understanding electromagnetic wave generation, scattering and coupling in plasma. Furthermore, relevant information can be inferred about the CME plasmoid structure, e.g., about the particle acceleration front geometry.

9.3 Low-Frequency Radio Diagnostics of Heliospheric Phenomena

The 3D structure of the Solar Wind can be derived from Interplanetary Scintillation Data (Hick and Jackson, 2001) provided by LOFAR (Best, 2007): - Large- and small-scale plasma structures can be outlined; - Fast and slow plasma streams can be identified and characterized; - Co-rotating interaction regions can be studied; - CME propagation and structure can be better described; - The response of the Geospace can be adequately mapped and quantified.

9.4 Low-Frequency Radio Diagnostics of the Earth's Ionosphere

LOFAR can probe the Geospace via riometric observations (Best, 2007) to provide: - The small- and large-scale state of the ionospheric plasma; - The ionospheric response to impinging solar electromagnetic and particle radiation; - The Ionosphere-Magnetosphere coupling features.

9.5 Conclusions

LOFAR is an innovative instrument for 3D tracking of radio sources from solar corona to the heliosphere and Earth's ionosphere. In particular, faint and

fast evolving features can be observed. Based on the effects of plasmas on electromagnetic wave propagation, refined diagnostics can be set up for inferring the spatial fine structure of the medium, keeping into account that turbulent scattering of em waves in plasma broadens the source size and sets a limit to the possibility to resolve fine structures (Bastian, 1995; Bastian, 2004). LOFAR key targets common to Solar, Solar-Terrestrial, Heliospheric, Magnetospheric and Ionospheric Physics are respectively: - Plasma turbulence; - Plasma response to various perturbations; - Particle acceleration; - Shock formation; - Shock propagation.

LOFAR plasma radio diagnostics together with complementary radio observations at higher frequencies and non-radio observations will provide new insights of the perturbative phenomenology of the Sun-Earth environment relevant to Space Weather applications through a significant improvement in the understanding of the physics of the phenomenology such as: - Precursors; - Triggers; - Onset; - Evolution; - Propagation; - Interactions.

Hence, a significant improvement of the reliability in Space Weather nowcasting and forecasting is expected. Furthermore, LOFAR will play the role of an enabling science ground-based facility for space-based observatory science (e.g. STEREO, Hinode, Solar Orbiter, etc.) The potential users are to be identified among the scientific communities involved in Heliospheric, Solar, Solar-Terrestrial, Magnetospheric and Ionospheric Physics as well as in Space Weather nowcasting and forecasting. In particular, a significant number of Italian scientists are actively involved in such research fields through various ground-based and space-based national and international projects. Worthwhile mentioning in this context is the newly started European COST Action ES0803 "Developing space weather products and services in Europe" (Belehaki et al., 2008), a cooperation in science and technology with the expected participation of more than twenty European countries among which Italy. In Italy, radio observations of the solar corona at metric and decimetric wavelengths have been routinely carried out at high time resolution (1 ms) and with accurate circular polarization measurements via the Trieste Solar Radio System (TSRS; <http://radiosun.oats.inaf.it>) operated by INAF (Messerotti et al., 2003b). TSRS acts as real-time data provider for the European Space

Weather Network (SWENET; <http://esa-spaceweather.net/swenet/>) and can detect SRBs affecting Global Positioning Systems (GPS) (Messerotti, 2008; Afrainovich et al., 2008), which is a fundamental issue in the light of the forthcoming European Global Navigation System Galileo. TSRS can profile geoeffective SRBs with the highest precision but with no spatial resolution. Hence joint observations with LOFAR could greatly improve its diagnostic capabilities when complementary 3D information on the associated triggering phenomenon become available. In fact, a better understanding of the underpinning physics is the only way to reliable prediction methods of SRBs occurrence, which does not exist to date.